

The Environment on few Mpc scales of Infrared Luminous Galaxies at Redshifts $z \sim 1$.

D. Marcillac¹, G. H. Rieke¹, C. Papovich^{1,2}, C. N. A. Willmer¹, B. J. Weiner¹, A. L. Coil^{1,3}, M. C. Cooper^{1,2,4}, B. F. Gerke⁴, J. Woo⁵, J. A. Newman^{3,6}, A. Georgakakis⁷, E. S. Laird⁷, K. Nandra⁷, G. G. Fazio⁹, J.-S. Huang⁹, D. C. Koo⁸

ABSTRACT

We investigate the environment of infrared luminous galaxies ($L_{IR}[8-1000 \mu\text{m}] > 10^{11} L_{\odot}$). We focus on the redshift range $0.7 \leq z \leq 1$, where these galaxies dominate the star formation activity and play a significant role in galaxy evolution. We employ MIPS $24\mu\text{m}$ data to identify infrared galaxies in the Extended Groth Strip (EGS). We use a local density indicator to probe the environment on few Mpc scales and a group member catalog, both of which make use of the DEEP2 spectroscopic redshift catalog, to quantify the environment of these galaxies.

We find that the local environment of LIRGs and ULIRGs is intermediate between that of blue and red galaxies. LIRGs and ULIRGs avoid underdense environments and inhabit local environments that are more dense on average than those of other DEEP2 galaxies at similar redshifts. However, when the comparison sample of the non-IR DEEP2 galaxies is restricted to have the same range of stellar mass, color, or luminosity as the IR-galaxies, there is no longer

¹Steward Observatory, University of Arizona, 933 N. Cherry Avenue, Tucson, AZ 85721

²Spitzer Fellow

³Hubble Fellow

⁴Department of Astronomy, University of California, Berkeley, CA 94720 – 3411

⁵Racah Institute of Physics, The Hebrew University, Jerusalem, Israel

⁶Institute for Nuclear and Particle Astrophysics, Lawrence Berkeley National Laboratory, Berkeley, CA 94720

⁷Astrophysics Group, Blackett Laboratory, Imperial College, Prince, Consort Rd, London SW7 2BZ, UK

⁸University of California Observatories/Lick Observatory, Department of Astronomy and Astrophysics, University of California, Santa Cruz, CA 95064

⁹Harvard-Smithsonian Center for Astrophysics, 60 Garden Street, Cambridge, MA 02138

any significant difference in environment; the IR-galaxies follow the same trends in the color-environment and luminosity-environment relations observed at $z \sim 1$.

We also find that about 30% of the LIRGs and ULIRGs belong to groups, associated with a minimum dark matter halo of $6 \times 10^{12} M_{\odot} h^{-1}$. The group members constitute 20 % of the sources responsible for the IR star formation rate density and comoving energy density at $z \sim 1$.

Subject headings: galaxies : evolution – infrared : galaxies – galaxies: starburst
– galaxies : general – galaxies : interactions

1. Introduction

The link between galaxy properties and environment has been studied extensively in the local Universe. For example, Oemler (1974) found that the late type galaxy fraction decreases with radius within a cluster, which is now known as the “*radius-morphology*” relation. Dressler (1980) extended this result to the “*density-morphology*” relation, showing that the fraction of morphological types is a function of the density in the local environment. This relation is found to hold in group and under-dense regions (Davis & Geller, 1976, Postman & Geller, 1984) and it appears to operate over several orders of magnitude in local density. Environment and galaxy properties such as colors, luminosity and physical parameters have also been studied thoroughly thanks to local surveys such as the Sloan Digital Sky Survey (SDSS, Blanton et al., 2003; Tanaka et al., 2004; Park et al., 2007). Gomez et al. (2003) show that the star formation rate (SFR) of galaxies is strongly correlated with the local projected galaxy density and defined a *density-SFR* relation, analogous to the *density - morphology* one. Clustering studies have given similar results (Zehavi et al. 2002 for the SDSS, and for the 2dF Galaxy Redshift Survey (2dFGRS), Colless et al., 2001; Norberg et al., 2001). Balogh et al. (2004) also show that the relative numbers of star-forming and quiescent galaxies vary strongly as a function of local density.

The link between environment and galaxy properties is now being extended to the distant Universe, thanks to deep multi-wavelength redshift surveys such as VVDS (VIMOS VLT Deep Survey, Lefevre et al., 2004), DEEP2 (Deep Extragalactic Evolutionary Probe, Davis et al., 2003, 2005, Faber et al., in prep.) and COSMOS (Scoville et al., 2006). The majority of the relations or trends found in the local universe have now been extended to higher z . Ilbert et al. (2006) found there is a strong dependence of the luminosity function on large scale environment up to $z \sim 1.2$. Cooper et al. (2006) show that the relations found in the local universe are still valid at $z \sim 1$: the local environment for red galaxies is more than 1.5 times denser than for blue ones. Galaxies with small [OII] equivalent width also occupy

regions of higher density. The relationship between galaxy over-density and rest-frame color at $z \sim 1$ also mirrors that seen in the local Universe. Cooper et al. (2007) find that the relationship between specific star formation rate and environment found at $z \sim 1$ is similar to the one found locally. Coil et al. (2007) studied the color and luminosity dependence of galaxy clustering at $z \sim 1$ and found similar results.

However, Elbaz et al. (2007) and Cooper et al. (2007) show that the relation between the total SFR and environment at $z \sim 1$ is inverted from that observed at $z \sim 0.1$: while in the local universe, the mean SFR of galaxies decreases in regions of higher over-density, at $z \sim 1$ it increases with local galaxy density. The nature of the infrared galaxy population also changes with redshift. In the local Universe, galaxies radiate $\sim 30\%$ of their bolometric luminosity over the 8-1000 micron range (Soifer & Neugebauer, 1991), but LIRGs¹⁰ and ULIRGs¹¹ are nonetheless rare locally and radiate only 6% of the integrated IR emission of local galaxies and $\sim 2\%$ of the local galaxy total bolometric luminosity (Soifer & Neugebauer, 1991, Sanders & Mirabel, 1996). However, this population has strongly evolved in number or luminosity at $z \sim 1$, where LIRGs are responsible for 70% of the comoving IR energy density; they dominate the star forming activity beyond $z \sim 0.7$ (Le Floc'h et al. 2005, Pérez-González et al. 2005). An important question is the link between LIRG/ULIRG evolution and the SFR-environment relation observed at $z \sim 1$.

In addition, we do not understand what causes the strong evolution of LIRGs and ULIRGs. Gas exhaustion undoubtedly plays a role (Bell et al., 2005). Galaxy environment may also be important. The connection of IR activity to galaxy morphology or merging has often been proposed for both local and distant LIRGs and ULIRGs (Hammer et al., 2005, Sanders et al., 1988). The local LIRGs and ULIRGs usually appear to have disturbed morphologies (Sanders & Mirabel, 1996). Ishida (2004) study a sample of 56 local LIRGs drawn from the IRAS Bright Galaxy Sample (Soifer et al., 1987) and find that all galaxies with $\log(L_{IR}/L_{\odot}) > 11.5$ show at least some evidence of tidal features. The majority of galaxies with $11.1 < \log(L_{IR}/L_{\odot}) < 11.5$ also tend to be disturbed, but $\sim 30\%$ are bright isolated spirals. In rough agreement, Wang et al. (2006) find that the fraction of interacting-merging galaxies and normal disk galaxies are respectively 48% and 40% among a sample of 159 local LIRGs detected in both the IRAS survey and the SDSS.

However, there are intriguing clues that the morphologies of IR galaxies may be different at $z \sim 1$. Several independent studies have shown that LIRGs tend to be associated with massive spirals at $z > 0.6$ rather than with interacting sources (Bell et al., 2005, Melbourne

¹⁰ LIRGs are classified as sources with $10^{11} \leq L_{IR} < 10^{12} L_{\odot}$.

¹¹ ULIRGs are classified as sources with $10^{12} L_{\odot} \leq L_{IR}$.

et al., 2005, Bridge et al., 2007, Lotz et al., 2006). However, Shi et al. (2006) used the very deep images from the UDF (HST Ultra Deep Field survey, Beckwith et al, 2005) and found that a significant fraction of the disk-dominated LIRGs show some signs of morphological disturbance or asymmetry. Bridge et al. (2007) also found that a significant fraction of sources classified as disk-dominated LIRGs show signs of disturbance or are in pairs. Taken together, these results suggest that the morphological properties of LIRGs may change with redshift.

Another approach is to test whether the LIRG properties arise from environmental effects, e.g., the density-SFR relation. Studies of the environment of LIRGs have not been very extensive, but they raise troubling questions. If so many local LIRGs and ULIRGs are triggered by galaxy interaction, then we might expect to find them predominantly in denser environments, groups or structures. However, this expectation is apparently not confirmed by the observations. Gonzalez-Solares et al. (2004) find a correlation length for the 3D infrared galaxy-galaxy autocorrelation function of $r_0 \sim 4.3 h^{-1} \text{Mpc}$ in the ELAIS (The European Large Area ISO Survey, Oliver et al., 2000, Rowan-Robinson et al., 2004) where $\bar{z} \sim 0.2$, consistent with the previous findings from IRAS (Saunders et al., 1992, Fisher et al., 1994). These results indicate weaker autocorrelations than are found for optical galaxies in the same redshift range from 2dFGRS or SDSS (Norberg et al., 2001, Zehavi et al., 2002). Owers et al. (2007) also find that starbursting sources tend to be less clustered on large scales (5-15 Mpc) compared to the overall 2dFGRS galaxy population. However, the local samples used in both cases are biased toward galaxies with L_{IR} below the LIRG range, and they could have different clustering properties (Gilli et al., 2007).

The environment of LIRGs and ULIRGs has not been studied extensively in the distant universe. Some works suggest that interactions might enhance IR activity at $z \sim 1$: Cohen et al., (2000) focused on sources in the HDFN (Hubble Deep Field North, Williams et al., 1996) detected at $15 \mu\text{m}$ with ISO ($\bar{z} \sim 0.63$) and showed that they are more clustered than average, with 90% of them lying within the redshift peaks. Lin et al. (2007) also find a mid-IR enhancement in pairs separated by less than a few tens of kpc in the EGS (Extended Groth Strip) region. Bridge et al. (2007) state that galaxies involved in a “merger process”¹² account for $\sim 60\%$ of the IR luminosity density at $z \sim 1$. However, none of these studies relies on a precise and systematic estimate of the galaxy local environment but rather on morphological or pair classification.

In this paper, we take advantage of the MIPS data obtained in the EGS in combination

¹²In close pairs, or classified as merging-interacting systems by visual inspection or using the CAS parameters (Conselice et al., 2003a, 2003b)

with other datasets in AEGIS (All-wavelength Extended Groth Strip International Survey, Davis et al., 2007) to study the local environment of LIRGs and ULIRGs at $0.7 < z < 1$. We will quantify the mean environment of these sources disregarding their morphology or pair classification. We explore whether their environment is significantly different compared to the other $R < 24.1$ galaxies at similar redshifts. In §2 we present the multi-wavelength data and environment catalogs that will be used through the paper. §3 presents the sample and its completeness limit and discusses how representative it is of the IR population. §4 addresses the issue of AGN contamination. §5 explores the SFR-density relation and expands the discussion of local environmental dependence for IR galaxies and other samples, and §6 address the link between IR galaxies and group membership. §7 discusses our results, which are summarized in §8. Throughout this paper, we assume $H_0 = 70 \text{ km s}^{-1} \text{ Mpc}^{-1}$, $\Omega_{\text{matter}} = 0.3$ and $\Omega_{\Lambda} = 0.7$; all the magnitudes are in the AB system; all the galaxy masses are stellar masses unless otherwise is stated.

2. The Data

This paper utilizes a subset of the AEGIS data described in Davis et al. (2007). The data sets relevant to our work are described in this section.

2.1. X-ray data

The EGS region has been observed by 8 ACIS-I pointings (Advanced CCD Imaging Spectrometer on *Chandra*) over $\sim 0.65 \text{ deg}^2$ with an exposure time of 200ks per pointing. The X-ray data reduction, source detection and flux estimation are carried out using methods described in Nandra et al. (2005). The $5\text{-}\sigma$ detection levels are 1.1 and $8.2 \times 10^{-16} \text{ ergs}^{-1} \text{ cm}^{-2}$ respectively in the soft (0.5 - 2.0 keV) and hard (2.0 - 7 keV) bands.

2.2. Spitzer/MIPS 24 μm data

The EGS was observed in January and June 2004 with MIPS (Multi-band Infrared Photometer for Spitzer, Rieke et al., 2004) on board the Spitzer Space Telescope as part of the *Spitzer* Guaranteed Time Observation (GTO) program. The observations were in the Slow Scan mode, which allows the coverage of large sky areas with high efficiency. The effective integration time at 24 μm is $\sim 1500 \text{ s}$ in the deepest part of the field, which is the main focus of this paper. The data were reduced with the MIPS Data Analysis Tool

(DAT, Gordon et al. 2005). The final mosaic has an interpolated pixel size of 1.245 " (half the native pixel scale) and covers $2.5 \times 0.2 \text{ deg}^2$. The point-spread function (PSF) at 24 μm is ~ 6 " in diameter and hence virtually all the detected sources are unresolved. The 24 μm catalog utilized PSF-fitting photometry done with DAOPHOT (Stetson, 1987), with procedures described in Papovich et al. (2004).

We use data from the deepest part of the field (0.35 deg^2), which coincides with the DEEP2 redshift survey. We used the approach of Papovich et al. (2004) to estimate the completeness of the data. Artificial sources were added to the images and extracted in the same way as real sources. The 50 and 80% completeness limits are estimated to be 50 and 82 μJy respectively. Papovich et al. (2004) also estimate the number of spurious sources as a function of 24 μm flux density in the Chandra Deep Field South, where their data have a similar total effective integration time and background as ours in the EGS. They show that at 82 μJy , the false detection rate should be less than 3% (see their Figure 1). The final astrometry has been checked against the DEEP2 photometric catalog of Coil et al. (2004). A systematic offset of 0.1" was found and removed. The remaining scatter relative to the DEEP2 photometric positions is estimated to be 0.6" at 1σ . Our final catalog includes 4417 sources with $f_{24} > 82 \mu\text{Jy}$.

2.3. Spitzer/IRAC data

IRAC (Fazio et al. 2004) data were also obtained under the GTO program in 2003 December and 2004 June/July. Dithered exposures in all four IRAC bands (3.6, 4.5, 5.8 and 8 μm) were taken at 52 positions for net exposures of ~ 2.7 hours per pointing. The data were initially processed to the basic calibrated stage using version 11 of the Spitzer Science Center pipeline. Custom IDL scripts were used to distortion-correct the individual frames, reject cosmic rays, remove other image artifacts, and project the frames onto a common reference frame for mosaicing. Identification of artifacts was facilitated because there were two data sets obtained at position angles rotated by $\sim 180^\circ$. The final mosaic is sub-sampled at 0.6" per pixel, half the native pixel size.

DAOPHOT/FIND was used to identify sources in the mosaics and to obtain their photometry. Because of source crowding, neighboring objects in a surrounding 200-pixel box were removed prior to obtaining photometry of a source in a 3" aperture. After applying aperture corrections, the source measurements were entered into two catalogs, one selected at 3.6 μm and containing about 73,000 objects, and the other selected at 8 μm with about 16,000 objects. The 5- σ detection limits are about 0.9, 0.9, 6.3, and 5.8 μJy respectively at 3.6, 4.5, 5.8 and 8 μm .

2.4. Spectroscopic Redshift Catalog

The EGS has been observed spectroscopically as part of the DEEP2 collaboration (Davis et al., 2003, 2007). Approximately 13500 spectra have been obtained so far in the EGS with DEIMOS, the multi-object spectrograph on the Keck II telescope (Faber et al., 2003). About 9500 of these redshifts are secure ($>95\%$ confidence), defined as having at least two spectral features detected at a significant level.

Details of the DEEP2 observations, catalog construction and data reduction can be found in Davis et al. (2003), Coil et al. (2004) and Davis et al. (2005). Sources targeted for spectroscopy are required to have $18.5 \leq R \leq 24.1$ and surface brightness $\mu_R \leq 26.5$. Stars and galaxies are distinguished using a combination of angular size, magnitude and position in color-color space; objects chosen for spectroscopy have at least a 20% probability of being a galaxy based on their photometry. Not all sources matching these criteria can be observed on slitmasks, due to their high number density. Therefore, various selection rules plus a final random selection are applied to pick sources for spectroscopy. The selection rules include a weight that is a function of both the R magnitude and the probability of being a galaxy. This color cut is used in the other (non-AEGIS) DEEP2 fields to select galaxies at $z > 0.75$ for spectroscopy. In the AEGIS field, galaxies at $z < 0.75$ are also selected but with a lower probability than a strict flux-limit would allow, which ensures a more uniform redshift distribution that is not peaked at $z = 0.5$. As a result, the observed density of galaxies at $z > 0.75$ in the AEGIS field is similar to other DEEP2 fields.

The DEEP2 survey is R-band-selected, which probes the rest-frame 4000 \AA at $z \sim 0.7$ and $\sim 3400 \text{ \AA}$ at $z \sim 1$. Therefore, at high redshift blue galaxies are preferentially selected. A bias against MIPS sources could result, since they are very dusty. However, part of this color bias is compensated by the intrinsic brightness of LIRGs and ULIRGs, which are among the brightest sources in this redshift range as a result of their strong star formation activity. The selection effects and biases in the DEEP2 data are discussed extensively in Gerke et al. (2005). Here we focus only on the $0.7 \leq z \leq 1$ redshift range, where these effects have been shown to be small.

2.5. Photometric Redshift Catalog

The EGS is also covered by one of the four fields from the Canada-France-Hawaii Telescope Legacy Survey (CFHTLS). The reduction and photometry of these images are described in McCracken et al. (2007, in preparation). The resulting catalog reaches a limiting

magnitude of $i'_{AB} \sim 26$. Photometric redshifts¹³ have been derived for objects with $i' \leq 24$ (Ilbert et al., 2006) using the *Le Phare* redshift code¹⁴, which provides a robust calibration method based on an iterative zero-point refinement combined with a template optimisation procedure and a Bayesian approach. VVDS provided thousands of redshifts to calibrate the photometric redshifts. They have an accuracy of $\sigma_{\Delta z/(1+z)} = 0.029$ with only 3.8% of the sources with $i'_{AB} \leq 24$ having $\text{abs}(\Delta z/(1+z)) \geq 0.15$ over the $0.2 < z < 1.5$ redshift range. Although useful to test for completeness, these redshifts are not accurate enough to be used to study the local environment of galaxies; as a comparison, $\text{abs}(\Delta z/(1+z))_{DEEP2} = 6.5 \times 10^{-5}$ at $z \sim 1$.

2.6. Environment Characterization

We characterize the environment of LIRGs and ULIRGs in two ways. The first is to estimate the local over-density around galaxies ($1 + \delta_3$, Cooper et al. 2005), which we use to probe whether IR-luminous galaxies tend to be located in over-dense regions compared with field galaxies. The second is to examine whether LIRGs inhabit preferentially galaxy groups (Gerke et al. 2005, 2007). These approaches give complementary insights about the environment of IR-luminous galaxies.

2.6.1. Local over-density estimator

We use the local over-density estimator described by Cooper et al. (2005, 2006). For each galaxy, a velocity interval of $\pm 1000 \text{ km s}^{-1}$ is defined around the object along the line of sight; galaxies outside this interval are excluded as foreground or background objects. All galaxies in the selected redshift range are projected to the redshift of the source. The local galaxy surface density, Σ_3 , is defined as the projected third-nearest-neighbor surface density. However this estimation only includes sources with accurate spectroscopic redshifts in DEEP2; Σ_3 varies as a function of redshift since both the sampling and the spectroscopic success and failures are functions of redshift. Therefore, for each density, Cooper et al. (2005) corrected Σ_3 for the variable redshift completeness of the DEEP2 survey and for the redshift dependence of the sampling rate. This correction is made by dividing each Σ_3 by the median $\langle \Sigma_3 \rangle$ of galaxies at this redshift in a redshift bin of $\delta z = 0.04$. Cooper et al.

¹³available on the Cencos database (Le Brun et al. 2007) at <http://cencos.oamp.fr/cencos/CFHTLS/>.

¹⁴www.lam.oamp.fr/arnouts/LE_PHARE.html

(2005) have verified the validity of this empirical correction on the DEEP2 Mock galaxy catalogs of Yan, White and Coil (2004). Dividing Σ_3 by the median value of $\langle \Sigma_3 \rangle$ leads to an estimate of the over-density relative to the mean density at a given redshift and will be noted as $1+\delta_3$ hereafter.

To minimize the impact of the survey edge, which could lead to biases in the local density estimator and properties, all galaxies within 1 h^{-1} co-moving Mpc of an edge of the surveys have been removed from our samples.

2.6.2. Group Catalog

Groups are defined here as bound structures, virialized associations of two or more observed galaxies. The algorithm to identify groups is presented in Gerke et al. (2005). The groups are identified using the Voronoi-Delaunay Method (VDM) originally implemented in Marinoni et al. (2002). The group-finding algorithm proceeds iteratively. In the first step, it identifies galaxies with a high density of neighbors; it next expands to a larger volume to compute a richness for the possible group. Finally, the richness estimate is corrected to account for the redshift-dependent number density of galaxies in the initial survey. This algorithm has also been calibrated using the mock catalogs of Yan, White and Coil (2004), which are designed to replicate the DEEP2 survey. Working with the mock catalogs, the algorithm is subject to significant systematic errors for putative groups with small velocity dispersions. However, it reproduces well the distribution of groups in redshift and velocity dispersion for velocity dispersions greater than 350 km s^{-1} (Gerke et al. 2005). In this paper we used a recent group listing from Gerke et al. (2007), where the algorithm was applied to a large dataset.

We will compare the IR properties of galaxies belonging to two samples, one in groups and the other in the field. The first one, hereafter *the group sample*, contains the galaxies belonging to groups with velocity dispersions greater than 100 km s^{-1} . We have decreased the velocity dispersion threshold from 350 km s^{-1} to 100 km s^{-1} and use the same prescription as Gerke et al. (2007) because of our emphasis on the properties of the galaxies and not the group properties. This new velocity dispersion threshold has been chosen because below it, the number of false detections of putative groups increases significantly. Gerke et al. (2005) estimate that the fraction of real group members that are successfully identified is $\sim 79\%$. This fraction does not vary much with velocity dispersion. The fraction of galaxies that are misidentified as group members in the resulting catalog is $\sim 46\%$. This level of contamination seems to be high; however, tests with mock catalogs show that the majority of galaxies in our group catalog truly belong to groups. In addition, all the results presented in section 5

would only be stronger with a less contaminated sample.

The meaning of “group” needs to be clarified. “Group members” means at least two group galaxies are detected in the DEEP2 sample. If we take into account the DEEP2 spectroscopic completeness limit, a very approximate real richness could be about 4 members; this estimate does not take into account errors by the group-finder algorithm. Coil et al. (2006) calculate the auto-correlation function of DEEP2 groups and estimate a minimum dark matter halo mass of $6 \times 10^{12} M_{\odot} h^{-1}$ for them. Assuming that the dark matter halo growth is close to a factor 2 between $z \sim 1$ and $z \sim 0$ (Sheth and Tormen, 1999) and using the dark matter halo mass – stellar mass relation that Yang et al. (2007) derived at $z \sim 0$ using SDSS galaxy groups, we find that the stellar mass of the dark matter halos of the DEEP2 groups is about $2 \times 10^{11} M_{\odot} h^{-1}$ at $z \sim 0$. This corresponds to a total stellar mass of \sim five M_{\star} galaxies, assuming $M_{\star} = 4 \times 10^{10} M_{\odot} h^{-1}$ (Bell et al., 2003).

The second sample, the *field sample* hereafter, is made of galaxies that do not belong to groups or belong to groups with a lower dispersion limit. Gerke et al. (2005) estimated that the fraction of misclassified group members represents only 6% of the reconstructed field sample, showing that the field sample is in fact dominated by field galaxies.

3. Defining a sample of LIRGs and ULIRGs.

We define here the sample of LIRGs and ULIRGs used in this paper and address how complete and representative it is.

3.1. Optical identification

The full MIPS 24 μm catalog has 4417 sources detected with $f_{24} > 82 \mu\text{Jy}$ (80% completeness limit) in the area where DEEP2 spectroscopy is available. We cross-correlate the MIPS catalog with the DEEP2 photometric catalog (Coil et al., 2004) for galaxies with magnitudes $R \leq 24.1$, using a search radius of $2''$. This step ensures a unique association between a 24 μm source and a secure spectroscopic redshift and avoids misassociations arising from the smaller number of sources in the redshift catalog. The search radius accounts for local astrometric uncertainties between the optical and 24 μm catalogs and allows for shifts in the brightest position of optical emission relative to the MIR peak (e.g., as in the Antennae galaxy, Mirabel et al., 1998). In the association process between the DEEP2 catalog and the MIPS sources, we find 2527 24 μm sources with unique counterparts down to $R = 24.1$. We rejected 219 associations because there was no unique optical identification. Of the 2527

associations, 1671 sources have a spectroscopic redshift with $z_q \geq 3$ corresponding to 38% of the total sample of MIPS sources and 66% of MIPS sources with an optical counterpart. See Table 1 for a summary of the different steps.

3.2. Sample definition

The flux limit of $f_{24}=82 \mu\text{Jy}$ ensures that the sample is complete for LIRGs up to $z \sim 1$, which we impose as the upper redshift limit (see Figure 6, discussed in more detail in Subsection 5.1). We exclude LIRGs at $z < 0.7$ to avoid contamination by lower redshift sources, which may have a different environment dependence than $z \sim 1$ sources. In addition, EGS spectroscopy is designed to probe the distant universe and only a small number of LIRGs with secure spectroscopic redshifts are found at lower redshifts (~ 80 with $z \leq 0.7$), which prevents us from building a good comparison sample of local LIRGs and ULIRGs. The final sample of LIRGs and ULIRGs is made of 314 sources with $0.7 \leq z \leq 1$ and $L_{IR} \geq 10^{11} L_{\odot}$.

3.3. Completeness of the Sample

At least two main issues affect the completeness of the sample: 1.) the spectroscopic redshift incompleteness; and 2.) the unknown redshift distribution of the $24 \mu\text{m}$ sources with $R > 24.1$. These two points are discussed below.

3.3.1. Spectroscopic redshift incompleteness

A part of the incompleteness for sources with $R \leq 24.1$ is due to the DEEP2 selection, which has only targeted a fraction of the sources with $18.5 \leq R \leq 24.1$ (see section 2.4). The probability for a source with $18.5 \leq R \leq 24$ to have been observed is estimated to be \sim

MIPS sources	#
MIPS sources with $f_{24} \geq 82 \mu\text{Jy}$	4417
MIPS sources with a unique counterpart with $R \leq 24.1$	2527
MIPS sources with a non-unique counterpart with $R \leq 24.1$	219
MIPS sources without any counterpart with $R \leq 24.1$	1671
MIPS sources with a unique counterpart with $R \leq 24.1$ and a reliable z_{spec}	1671

Table 1: Optical identification of the MIPS sources.

0.63. Another issue is the DEEP2 *failures*, which are the sources that were targeted but for which no secure spectroscopic redshift was obtained. These represent $\sim 30\%$ of the sample of targeted sources. As a consequence, the overall completeness of the DEEP2 sample is $\sim 44\%$ over the 0.7-1.3 redshift range, assuming the failures are uniformly distributed in z .

However LIRGs and ULIRGs are generally optically brighter than the field sources, have emission lines, and are relatively blue galaxies (according to the bimodality definition in Willmer et al., 2006). Some blue failures have also been targeted with LRIS-B and the great majority of them tend to have $z > 1.4$ (Willmer et al., 2006, C. Steidel, 2004, private communication). Since we have restricted our sample to the $0.7 \leq z \leq 1$ range, the completeness should be higher. In addition, the fraction of DEEP2 failures for sources with a similar R-I color as LIRGs and ULIRGs is close to 25%, which is lower than the mean failure rate.

To improve the completeness estimate of our sample, we use the photometric redshifts of CFHTLS. The CFHTLS only covers $\sim 70\%$ of the EGS field and we are only able to include 3163 of the 4417 MIPS sources. The MIPS source and photo- z catalogs were matched with a $2''$ search radius. Unique associations are found for 2187 $24 \mu\text{m}$ sources¹⁵, among which 1717 have a secure photo- z .

Since photometric redshifts rely more on the spectral shape and the presence of the Balmer break, they are less reliable for objects with intense starbursts. Emission lines associated with starbursting galaxies and bright enough to affect the photometry are not incorporated in an accurate way in the SED templates. IR sources are also affected by extinction. For all these reasons, we have tested the accuracy of the photometric redshifts of the IR sources. This test is based on the 787 galaxies with DEEP2 spectroscopic redshifts with $z_q \geq 3$ among the $24\mu\text{m}$ sources. The comparison of the two redshifts is presented in Tables 2 and 3 and Figure 1 for $z < 0.7$, $0.7 < z < 1$ and $z > 1$ bins. We find that the photometric redshift is typically 50% less accurate for IR sources than for the whole sample and that the rate of catastrophic errors ($\eta = \sigma_{\Delta z / (1+z)} > 0.15$) is twice as large. These results are in agreement with those found for starbursting sources in Ilbert et al. (2006). Despite the photometric redshifts being less accurate for IR sources, the uncertainties are small enough to use them to estimate the completeness of the LIRG and ULIRG sample over $0.7 \leq z \leq 1$; however, they will not be used for the environment study in the following sections. The sample of LIRGs defined in section 3.2 represents $\sim 57\%$ of the LIRGs with a photometric redshift in the same redshift range and with $18.5 < R \leq 24.1$. This completeness level is significantly higher than that for the full EGS DEEP2 sample. We have also used

¹⁵This fraction is similar to that found when matching the $24\mu\text{m}$ catalog to the DEEP2 photometric catalog.

the photometric redshifts to estimate the completeness of the overall DEEP2 survey for $0.7 \leq z \leq 1$ and $18.5 \leq R \leq 24.1$, independent of infrared detections, and find 53% of the sources with $0.7 \leq z_{phot} < 1$ and $18.5 \leq R \leq 24.1$ have a spectroscopic redshift in the same range. The difference between the two completeness results (53 and 57%) might be due to the uncertainties in the photometric redshifts, $\sigma_{\Delta z/(1+z)} = 0.029$, which becomes $\sigma \sim 0.06$ at $z=1$.

3.3.2. Redshift range of the sources with $R > 24.1$

There are 1671 sources detected with MIPS at $24 \mu\text{m}$ that do not have counterparts with $R \leq 24.1$. These sources represent approximately 38% of the $24\mu\text{m}$ sample and could significantly affect our conclusions if they fall in the $0.7 \leq z \leq 1$ range. Sources that are optically faint and IR bright have been studied with IRS (Houck et al., 2005, Yan et al., 2007, Weedman et al. 2006). These extreme sources are mainly found at $z > 1$. However, the sources in our sample are ~ 10 times fainter at $24 \mu\text{m}$ than these high redshift sources.

Since we cannot compute photometric redshifts based on the optical data for such faint sources, we used the IRAC colors to measure the wavelength of the so called “stellar bump” and estimate a rough fraction of sources with $z \leq 1$. This broad feature is associated with the spectral peak at $\sim 1.6 \mu\text{m}$ caused by red giant and super-giant stars; it can provide a rough photometric redshift estimate if the stellar component dominates at the NIR wavelengths (Simpson & Eisenhardt 1999, Le Floch et al., 2004). Weedman et al. (2006) use this bump in addition to the optical criterion $m_r > 23$ to pre-select “starbursting sources” at high redshift for IRS observation. The IRS spectra show that except for one object at $z=0.98$, all of the selected sources are at $z \sim 1.5-2$.

To estimate the redshifts, we first cross-correlated the optically faint MIPS sources with the IRAC data. There are 1260 MIPS sources with a unique counterpart out of the 1373 MIPS sources that are located in the IRAC field. Among them, $\sim 41\%$ and 33% of the sample tend to exhibit a “stellar bump” around $\sim 4.5 \mu\text{m}$ (channel 2) and $\sim 5.8 \mu\text{m}$ (channel 3), respectively, giving a crude redshift range estimation of $z \sim 1.8$ and ~ 2.5 . 15% of the

	$\sigma_{\Delta z/(1+z)}$	$\eta = \sigma_{\Delta z/(1+z)} > 0.15$
IR sources	0.043	6.2%
whole sample ¹	0.029	3.8%

Table 2: Accuracy of the photometric redshifts for the LIRG and ULIRG sources compared to that for the whole sample of photometric redshifts for the CFHTLS.

Comments : (1) from Ilbert et al. (2006)

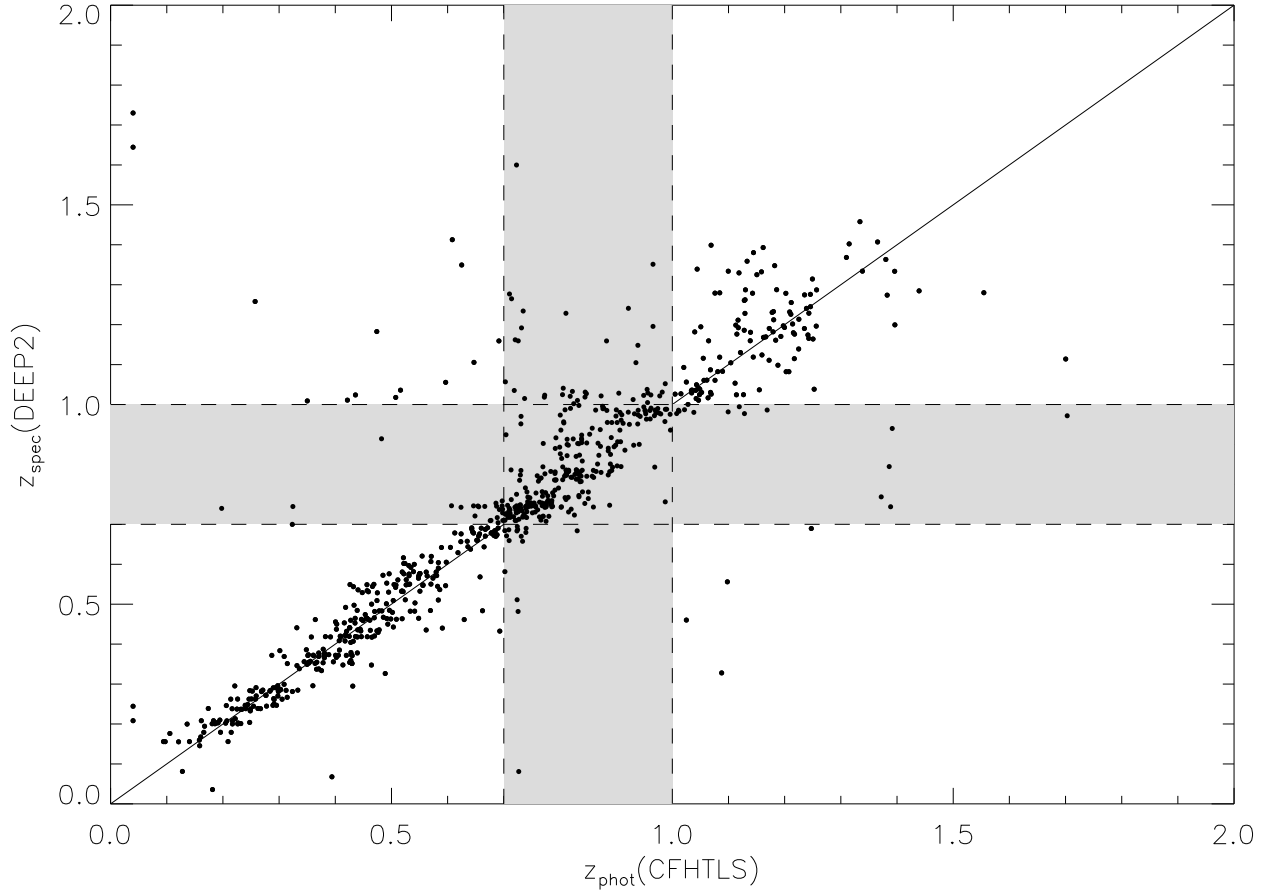


Fig. 1.— Comparison between the photometric and spectroscopic redshifts from CFHTLS and DEEP2 respectively for sources detected at $24\ \mu\text{m}$ above the $82\ \mu\text{Jy}$ completeness limit. The dashed lines and grey area show the redshift range we focus on. Despite the photometric redshifts being less accurate for IR sources, the uncertainties are small enough to use them to estimate the completeness of the LIRG and ULIRG sample over $0.7 \leq z \leq 1$.

	$z_{DEEP2} < 0.7$	$0.7 \leq z_{DEEP2} < 1$	$1 < z_{DEEP2}$
$z_{CFHTLS} < 0.7$	89 %	7 %	4 %
$0.7 < z_{CFHTLS} \leq 1$	5 %	83 %	12 %
$1 < z_{CFHTLS}$	3 %	10 %	86 %

Table 3: Accuracy of the CFHTLS photometric redshifts for LIRG and ULIRG sources as a function of redshift.

remaining sources exhibit a power law SED in the IRAC bands; such sources have been studied in the CDFS and tend to be at $z > 1$ (Alonso-Herrero et al.; 2006; Donley et al.; 2007; Papovich et al.; 2007). 7% show a stellar bump compatible with being at $3.6 \mu\text{m}$ or lower wavelength and could be sources at $z \sim 1.2$ or below. The rest of the sample cannot be classified. These sources exhibit a decrease in the IRAC SED from 3.6 to $5.8 \mu\text{m}$ and an increase at $8 \mu\text{m}$. This can be interpreted as sources for which the PAH emission band at $6.2 \mu\text{m}$ is detected at $8 \mu\text{m}$. If this interpretation is right, these sources could be at a $z < 1$. As a consequence, between 4 to 11% of the optically faint sources could be at $z < 1$.

3.4. Is the “LIRG and ULIRG” sample unbiased?

Since our LIRG and ULIRG sample is not complete, we need also to test how representative it is. Due to the high density of sources that satisfy the DEEP2 criteria required for a source to be targeted, various selection rules plus a final random selection were applied among multiple candidates to fill the DEIMOS slit masks (see Subsection 2.4). None of these criteria should introduce a strong bias in the sample of IR sources. To check, we compare the color-magnitude distribution in Figure 2 for the sources with $18.5 < R < 24.1$ for which the CFHTLS gives $0.7 \leq z_{\text{phot}} < 1$ (open black circles) to the spectroscopic sample of LIRGs and ULIRGs. Figure 2 shows that the spectroscopic sample of galaxies used in this work covers the same parameter space as the larger DEEP2 parent sample.

4. AGN contamination

IR galaxies are known to be powered by both AGN and star formation activity. It is not known whether galaxies dominated by AGN will lie in similar environments as star-forming ones. We use X-ray and IRAC data to isolate X-ray detected AGN and IRAC power-law ones to estimate the AGN contamination of our sample.

4.1. MIPS sources with X-ray emission

X-ray data are a primary way to identify AGN activity. We matched the X-ray catalog with the optical counterparts of the LIRGs because the astrometry is better for the optical. The PSF of Chandra is not uniform over the field of view, varying from $\sim 0.5''$ (FWHM) at the center, increasing up to $4''$ (FWHM) close to the edge. The search radius for the X-ray optical correlation has been changed adaptively as a function of the off-axis angle to account

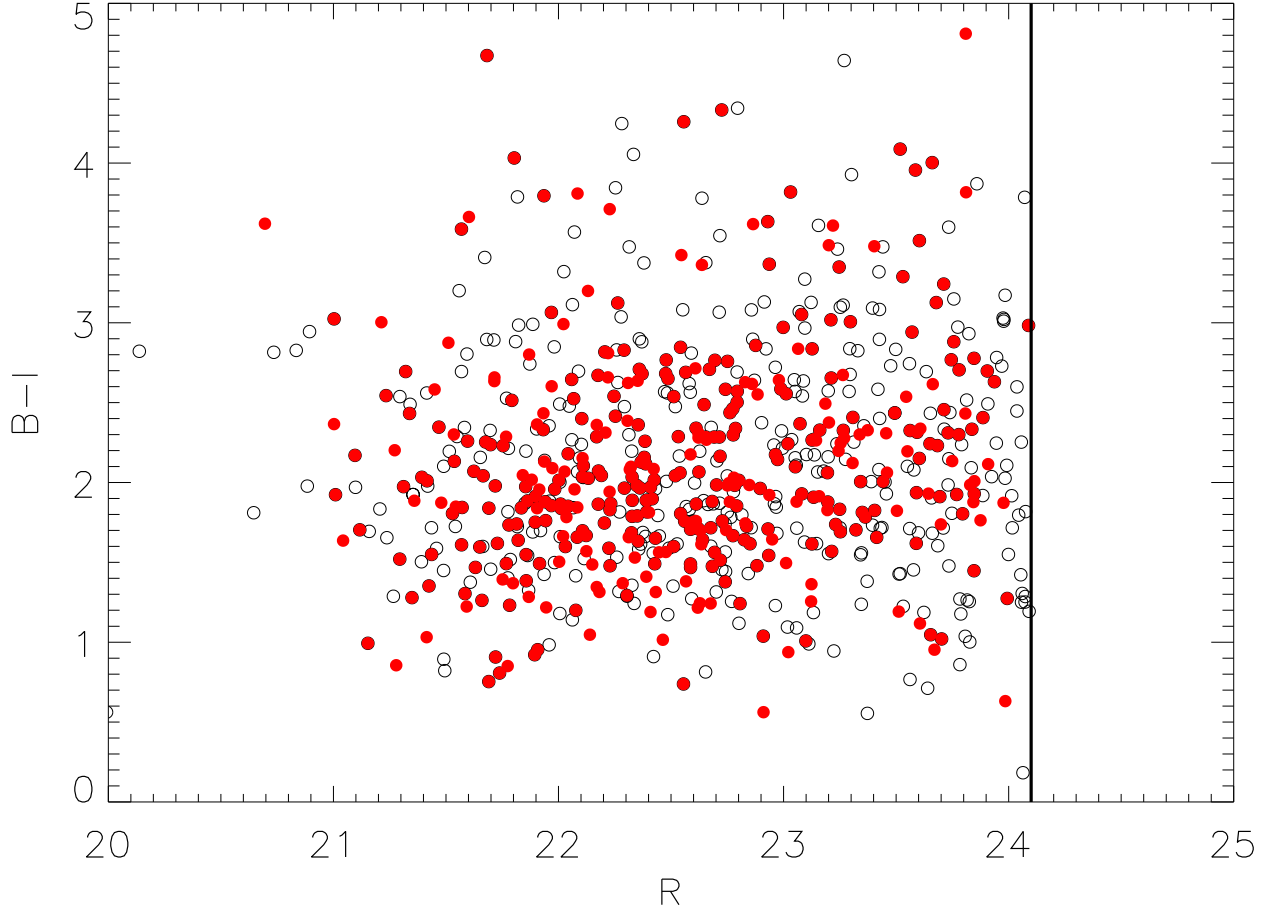


Fig. 2.— B-I color as a function of R for IR-galaxies with $0.7 \leq z_{\text{phot}} \leq 1.0$ (open black circles) and IR-galaxies with $0.7 \leq z_{\text{spec}} \leq 1.0$ (red solid circles). The vertical line is the $R=24.1$ DEEP2 magnitude limit. The plot shows that both samples cover a similar range in apparent magnitude and color suggesting there is no bias in the spectroscopic sample. [See the electronic edition of the *Journal* for a color version of this figure.]

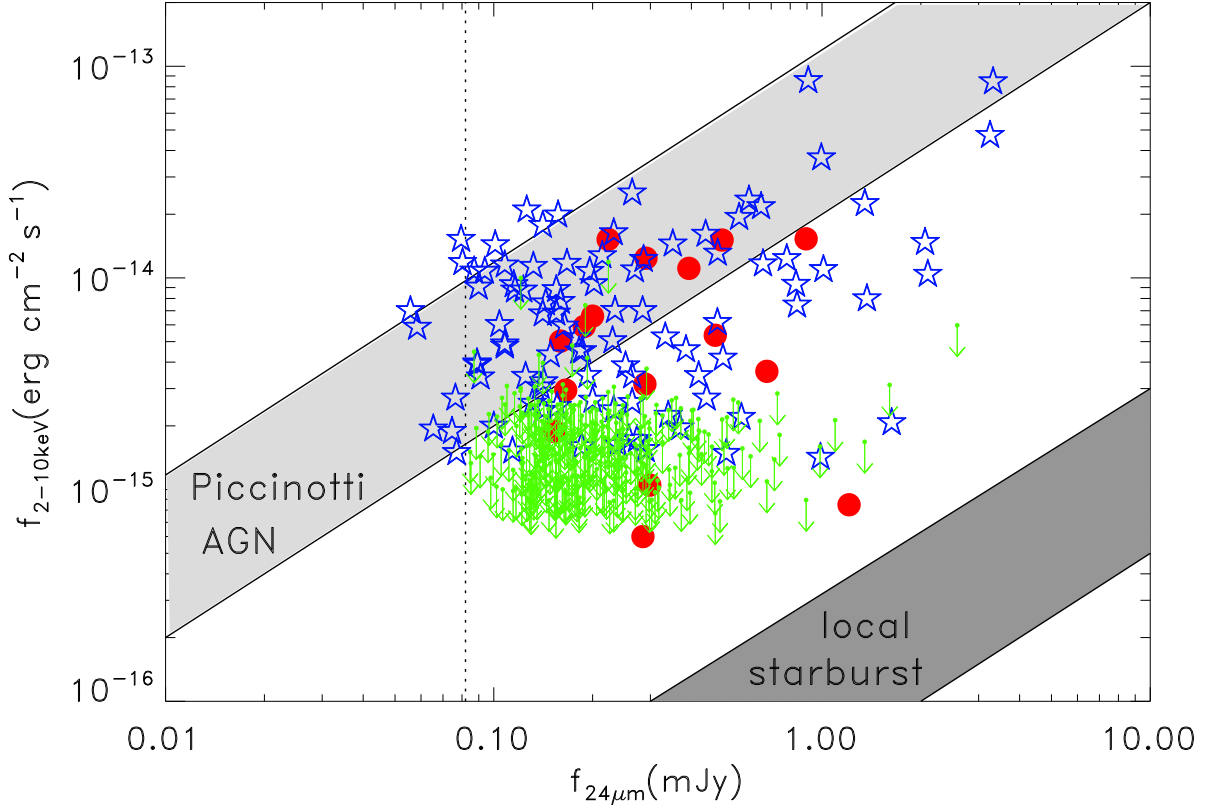


Fig. 3.— f_{24} as a function of the X-ray flux in the hard band. **Solid red circles** : Sources detected in the hard X-ray band. **Open blue stars** : X-ray sources detected in the 1 M sec field in the CDFS with a $24 \mu\text{m}$ counterpart (Rigby et al. (2004)). **Green arrows** : IR-galaxies with an X-ray upper limit. The lightly shaded area is the extrapolation of the median X-ray to mid IR ratio of local hard X-ray selected AGN (Piccinotti et al., 1982) while the dark shaded area is an extrapolation of the local starburst relation from Ranalli et al. (2003). The extrapolation is described in Alonso-Herrero et al. (2006). The dashed line is the MIPS completeness limit. This figure shows that the AGN contamination is weak as seen from the distribution of upper limits represented by the green arrows. [*See the electronic edition of the Journal for a color version of this figure.*]

for this effect. Figure 3 presents the 24 μm flux versus the 2-10 keV X-ray flux of the LIRGs detected in the X-ray hard band (red solid circles) or the upper limits of undetected sources (green arrows). The lightly shaded area represents the extrapolation of the median X-ray to mid IR ratio of local hard X-ray selected AGN (Piccinotti et al., 1982) while the dark shaded area is an extrapolation of the local starburst relation from Ranalli et al. (2003)¹⁶. A total of 20 LIRGs are detected with at least one measurement in one of the X ray bands (17 in the soft band, 16 in the hard band and 14 in the ultra hard one), which leads to a contamination of $\sim 6\%$ of the LIRG and ULIRG sample. Twenty other sources have upper limits falling within the Piccinotti et al. (1982) region and could be AGN, which gives an upper limit of $\sim 12\%$ for the AGN contamination.

One could argue that the X-ray data in the EGS are not deep enough and that as a result we miss some dusty AGN. Therefore, we also show the distribution of the hard X-ray sources with MIPS counterparts at 24 μm in the CDFS (Rigby et al., 2004, blue stars). Most of the AGN from Rigby et al. (2004) are X-ray brighter than the majority of the X-ray upper limits of the LIRGs studied here indicating that we must have missed relatively few AGN when compared to the deepest X-ray fields.

4.2. IRAC color selection

The IRAC colors have been used extensively to find dusty active galaxies not detected in the X-ray (Lacy et al., 2004, Stern et al., 2005, Alonso-Herrero et al., 2006, Barmby et al., 2006, Donley et al., 2007). An object dominated by a dusty AGN will show little sign of the stellar bump and its IRAC SED will be fitted by a red power law with $f_\nu \propto \nu^\alpha$ where $\alpha < 0$. The range of α allowed to define power-law AGN varies and can be defined as $\alpha < -0.5$ (Donley et al., 2007, Alonso-Herrero, 2006) or $\alpha \leq 0$ (Barmby et al., 2006). One of the reasons to choose a stricter definition (e.g., $\alpha \leq -0.6$) for the power law sources is that the redshift range of these sources is usually unknown and the goal is to ensure the sources selected are really dominated by a power-law AGN. In our case, the redshift range of the sources is known and we can reasonably expect sources with an IRAC SED fitted with $-0.5 \leq \alpha < 0$ to be dominated or partly powered by an AGN. We also want to estimate an upper limit on the contamination by the IRAC power-law sources in our sample, so we will consider both ranges of α . Five sources are found with $\alpha \leq -0.6$, while 11 are found with $\alpha \leq 0$ among the 283 LIRG sources with a detection in all the IRAC bands. The small number of power-law sources detected in this sample is not very surprising since a large fraction of the power-law sources is found at

¹⁶See Alonso-Herrero et al., 2004 for more details

higher redshift (Alonso-Herrero, 2006, Donley et al., 2007, Papovich et al., 2007). Among these 11 sources, 5 are X-ray detected in the hard band, which shows that these techniques of selecting AGN are complementary.

4.3. AGN contamination among the LIRGs and ULIRGs

At low redshift, La Franca et al (2004) show that at least 25% of the MIR sources detected in the ELAIS-S1 field are associated with an AGN according to their optical spectra; they stress that this percentage is a lower limit since some objects whose spectra do not show signs of AGN activity are detected in the X-ray. However, the presence of an AGN does not imply that it dominates the total infrared luminosity. Using SED modeling, Rowan-Robinson (2005) showed that the total infrared luminosity is dominated by AGN activity for only 11% of the total ELAIS sample.

In the redshift range we are studying, Fadda et al. (2002) combine X-ray with MIR $15\mu\text{m}$ data in the Lockman Hole and HDFN to conclude that the AGN contribution is about 17% of the $15\mu\text{m}$ background. Liang et al. (2004) studied the optical emission lines and conclude that about 23% of the LIRGs detected at $15\mu\text{m}$ are associated with AGN. Weiner et al.(2007) studied the AGN contamination of all the DEEP2 galaxies in the $0.35 < z < 0.81$ redshift range in the pseudo-BPT diagram (independent of the MIR detections) and find that 2-3% of the blue galaxies with emission lines could still be dominated by AGN, while 1/3 of the red galaxies with emission lines are close to the star-forming track, where blue and red galaxies are defined in Willmer et al. (2006). Combining these results for LIRGs and ULIRGs, we find that $\sim 13\%$ of the sample could be contaminated by AGN. However, since the red LIRGs are bluer than most of the red sequence, this estimate of AGN contamination may be high.

However, even if AGN activity is detected, the star-formation activity can still dominate the IR luminosity of these sources (Oliver & Pozzi, 2005, Rowan-Robinson, 2005, Le Floc'h et al., 2007). Because of the uncertainty in the main engine of the IR emission, we have not removed these sources from the sample, but we have checked that their removal does not change our conclusions.

5. Quantifying the local environment of LIRGs and ULIRGs.

The goal of this section is to probe whether LIRGs at $z \sim 1$ are found preferentially in over-dense or under-dense environments. We use the local environment indicator δ_3 defined

in section 2.6.1 and refer to it as the quantity $D = \log_{10}(1 + \delta_3)$.

5.1. SFR(IR)–local density relation.

The total infrared luminosity (L_{IR}) is derived using the 24 μm data. The continuum of the mid-infrared emission of galaxies is dominated by the output of the very small grains (VSG, Desert, Boulanger & Puget, 1990). To this continuum must be added broad aromatic emission features at 6.2, 7.7, 8.6, 11.3 and 12.7 μm (PAH, Puget & Leger, 1989). At $z < 0.6$ the 24 μm emission probes the VSG continuum, which has been shown to correlate very well with L_{IR} (Chary & Elbaz, 2001, Alonso-Herrero, 2006). At higher redshifts and up to $z \sim 1.2$, the 12 μm PAH complex enters the MIPS 24 μm band. The luminosity at 12 μm has also been shown to correlate well with the L_{IR} in the local universe (Chary & Elbaz, 2001) and up to $z \sim 1.2$ (Marcillac et al., 2006).

We estimate the infrared luminosity of each galaxy using the spectral energy distribution (SED) from the Dale & Helou (2002) library as explained in Marcillac et al. (2006). Each of the template SEDs is redshifted to match the galaxy. Then, the SED with MIR flux density closest to the observed value is used to derive L_{IR} after it is normalized to the exact observed flux density. Marcillac et al. (2006) compared L_{IR} estimated using 24 μm data to L_{IR} estimated using radio data for LIRGs and found a scatter of 40% between the two estimates. Using stacking analysis (Papovich et al., 2007) or direct FIR detection (Frayser et al., 2006) it appears that the FIR emission of distant IR sources is in agreement with SED templates, which are calibrated on local IR sources, up to $z \sim 1$.

Figure 4 shows the evolution of L_{IR} with z ; The grey area shows the trend of the completeness limit of the IR luminosity with redshift. For LIRGs and ULIRGs, the star formation is dominated by the infrared emission (Bell et al., 2005) and we use the relation of Kennicutt (1998) to estimate the SFR from L_{IR} . scenarios and galaxy evolution has often been discussed for local and distant LIRGs and ULIRGs (Hammer et al., 2005, Sanders et al., 1988). Figure 5 presents the local environment of the IR galaxies as a function of L_{IR} . We have divided this figure into 4 luminosity bins: the first three are designed to have approximately the same number of objects (~ 100), while the last is made of ULIRGs and the brightest LIRGs. The red squares are the median values in each bin and the error bars are a $1-\sigma$ dispersion estimated on each side of the median value. The figure shows that there is no strong dependence between L_{IR} and the local density up to $L_{IR} \sim 7-8 \times 10^{11} L_{\odot}$. This result suggests that once a galaxy becomes a LIRG or a ULIRG, it is unlikely that the environment has a significant influence on the SFR activity in a substantial number of sources, at least in or near the dense environments that are probed in the EGS. This is in accordance with results

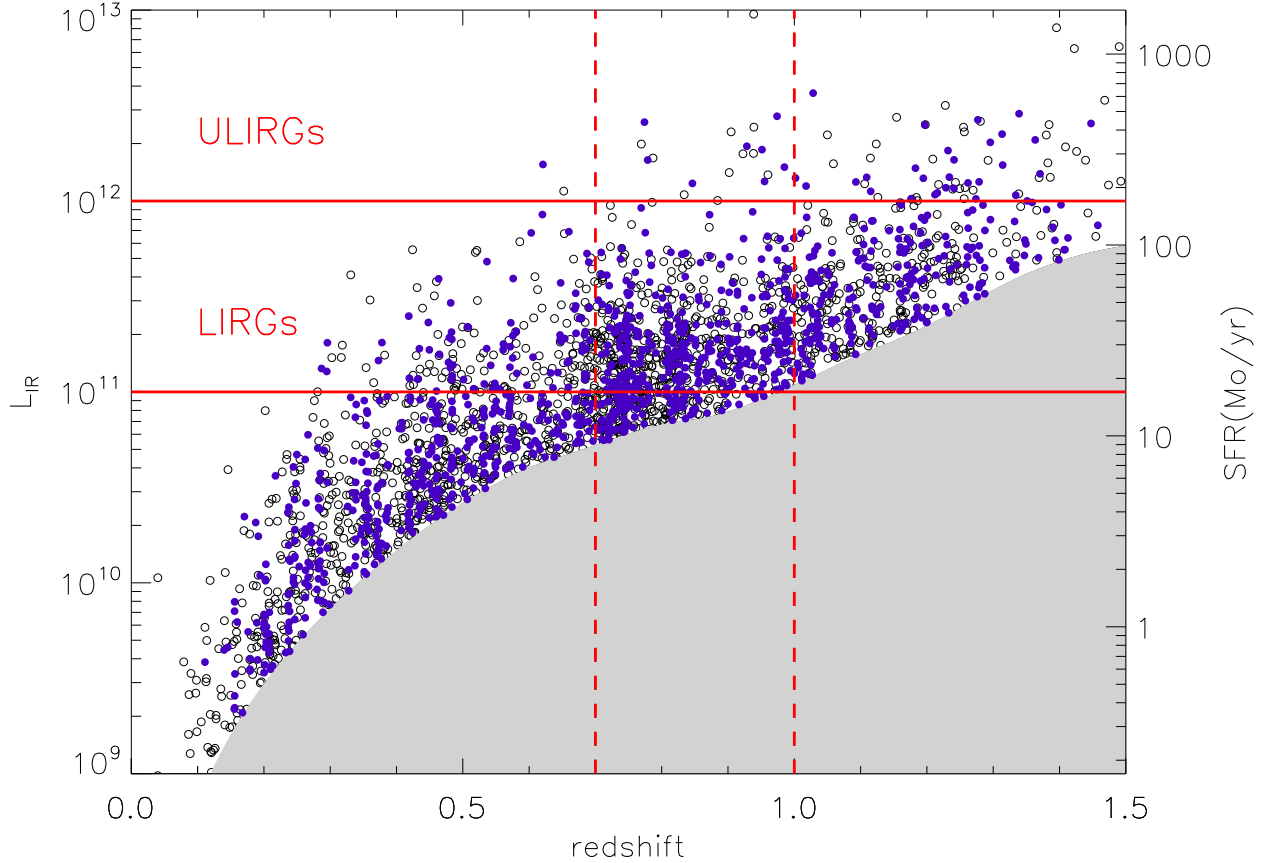


Fig. 4.— Total infrared luminosity as a function of redshift for sources above the MIPS completeness limit of $82 \mu\text{Jy}$ (grey region). **Solid blue circles** : sources with a secure spectroscopic redshift in DEEP2. **Empty circles** : sources with photometric redshift. The red dashed lines show the redshift range where we focus. The star formation rates in units of solar masses per year, $\text{SFR}(\text{IR})$ were derived using the relation of Kennicutt (1998) : $\text{SFR}(\text{IR}, M_{\odot}/\text{yr}) = 1.71 \times 10^{-10} (L_{\text{IR}}/L_{\odot})$. **Red solid lines** : show the LIRG and ULIRG regimes.

found in the local universe where the star-forming sources (with $EW(H\alpha) > 4\text{\AA}$) do not show any correlation between EW and local environment density (Balogh et al., 2004). scale to prevent us from finding a trend. For example mergers of galaxies could help consume the gas very quickly, feeding both an AGN and an intense burst of star formation. However, only a small fraction of LIRGs and ULIRGs at $0.7 < z < 1$ are associated with direct mergers and it is now accepted that the majority of LIRGs exhibit only slightly disturbed morphology, which tend to rule out this hypothesis.

At $\log_{10}(L_{IR}) \geq 11.9$, there is only one object in an under-dense environment ($\log_{10}(1+\delta_3) < 0$), whereas 8 sources lie in over-dense environments. One of these has an AGN since it is detected in all the X-ray bands and another is classified as an IRAC power law object. The other sources do not have any AGN signature in the X-Ray or IRAC but a dusty AGN can not be excluded. Therefore, ULIRGs tend to be found in over-dense environments; this conclusion is weakened by the small number of ULIRGs in this field. We used Monte Carlo simulations to estimate the significance of this tendency. We use the whole sample of LIRGs (without ULIRGs) and find a probability of $\sim 15\%$ to have 5 of 6 sources in overdense environments. This result is in agreement with Lin et al. (2007) who find a mid-IR enhancement in pairs separated by less than a few tens of kpc (Lin et al. 2007) for ULIRGs.

However, there is another possible explanation since the sources with $\log_{10}(L_{IR}) \geq 11.9$ are also optically brighter ($M_B = -21.43^{+0.48}_{-0.56}$) than the ones fainter in the IR ($M_B = -20.64^{+0.71}_{-0.53}$). The optically brighter sources are also in denser environments at $z \sim 1$ (Cooper et al., 2007). As a consequence, the fact that the local environment of ULIRGs tends to be denser can be interpreted with the density - luminosity relation alone since ULIRGs tend to have a similar environment to sources without IR detection and similar optical luminosity.

5.2. Comparing the local environment of LIRGs and ULIRGs with that of $0.7 \leq z \leq 1$ optically ($R \leq 24.1$) selected galaxies

We therefore compare the environment of LIRGs and ULIRGs to that of non-IR-emitting optically-selected galaxies at similar redshift. The distribution of $D = \log(1+\delta_3)$ for the “LIRG and ULIRG” sample is presented in Figure 6 (red histogram). We find that LIRGs and ULIRGs tend to be in over-dense environments, since $\langle D_{LIRG\&ULIRG} \rangle = 0.12$, which is also

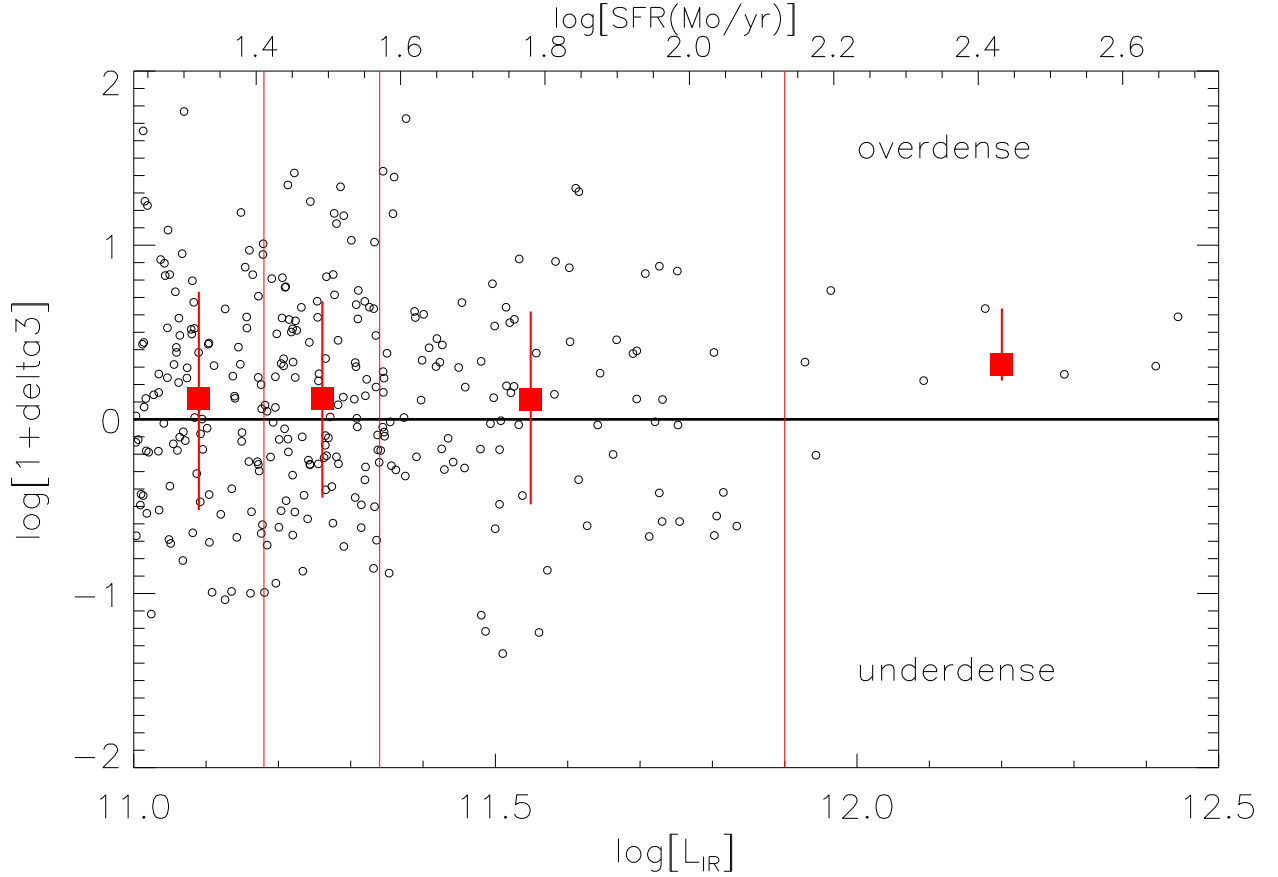


Fig. 5.— Local environment of LIRGs as a function of L_{IR} . The data have been divided into four bins : the first three are designed to approximately contain the same number of objects (~ 100), while the latter is made of ULIRGs and the brightest LIRGs. The red squares are the median values in each bin and the error bars are a $1-\sigma$ dispersion estimated on each side of the median value. [See the electronic edition of the Journal for a color version of this figure.]

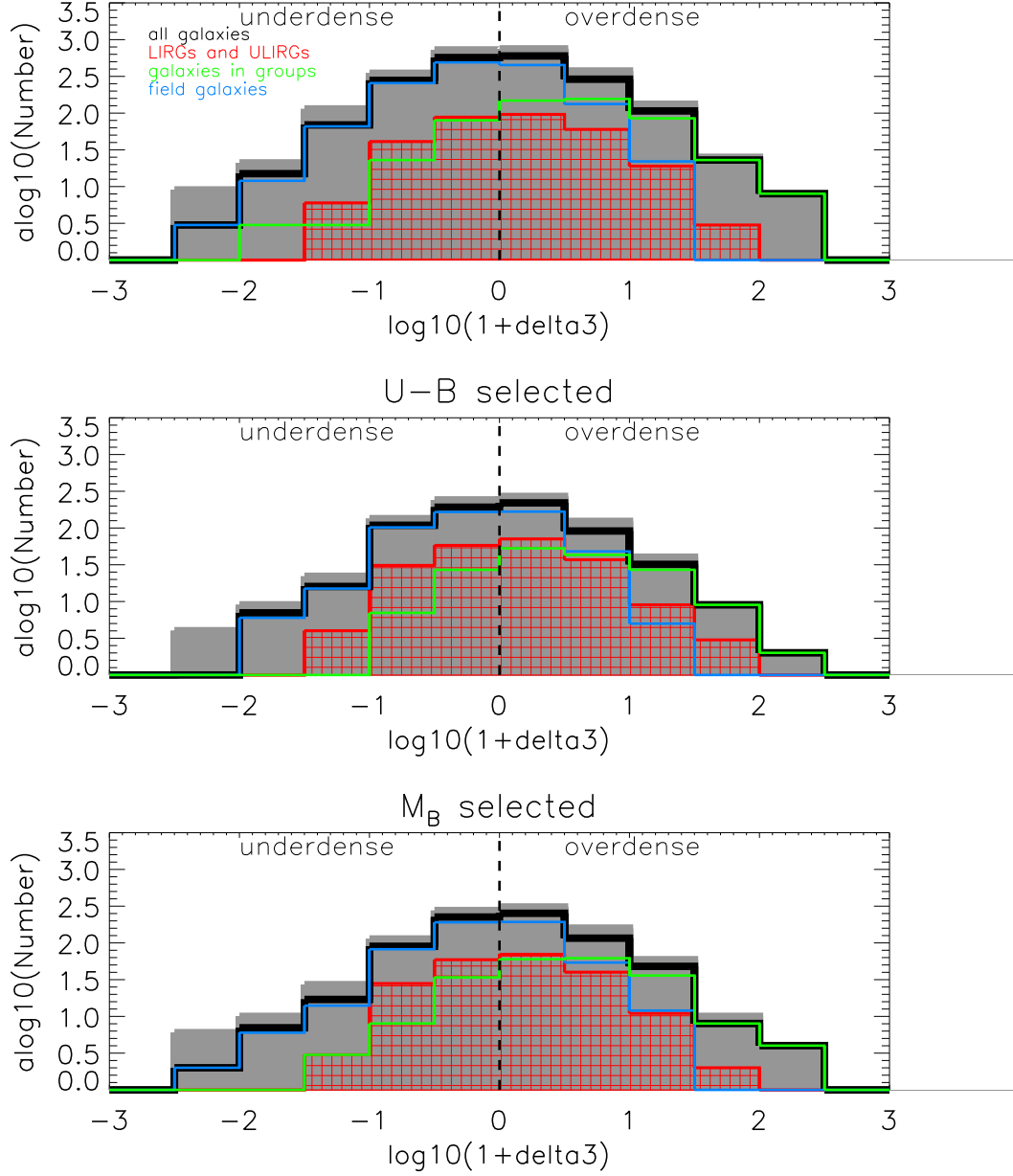


Fig. 6.— Comparison of the local environment of the LIRG and ULIRG sample (red) with the “all galaxy” sample (grey area). The sources classified in Gerke et al. (2007, black) have been divided into two categories : the “group” sample, which is composed of sources belonging to groups with $V_{\text{disp}} > 100 \text{ km s}^{-1}$ (green), and field sources (blue). **Top** : The samples are composed of all the sources with $0.7 < z < 1$. **Middle** : The samples are composed of sources with $0.7 \leq z \leq 1$ and $0.70 \leq U-B \leq 1.04$ which is the color range of the LIRGs and ULIRGs. **Down** : The samples are composed of sources with $0.7 < z < 1$ and $-21.18 \leq M_B \leq -19.93$ which is the absolute magnitude range of the LIRGs and ULIRGs.

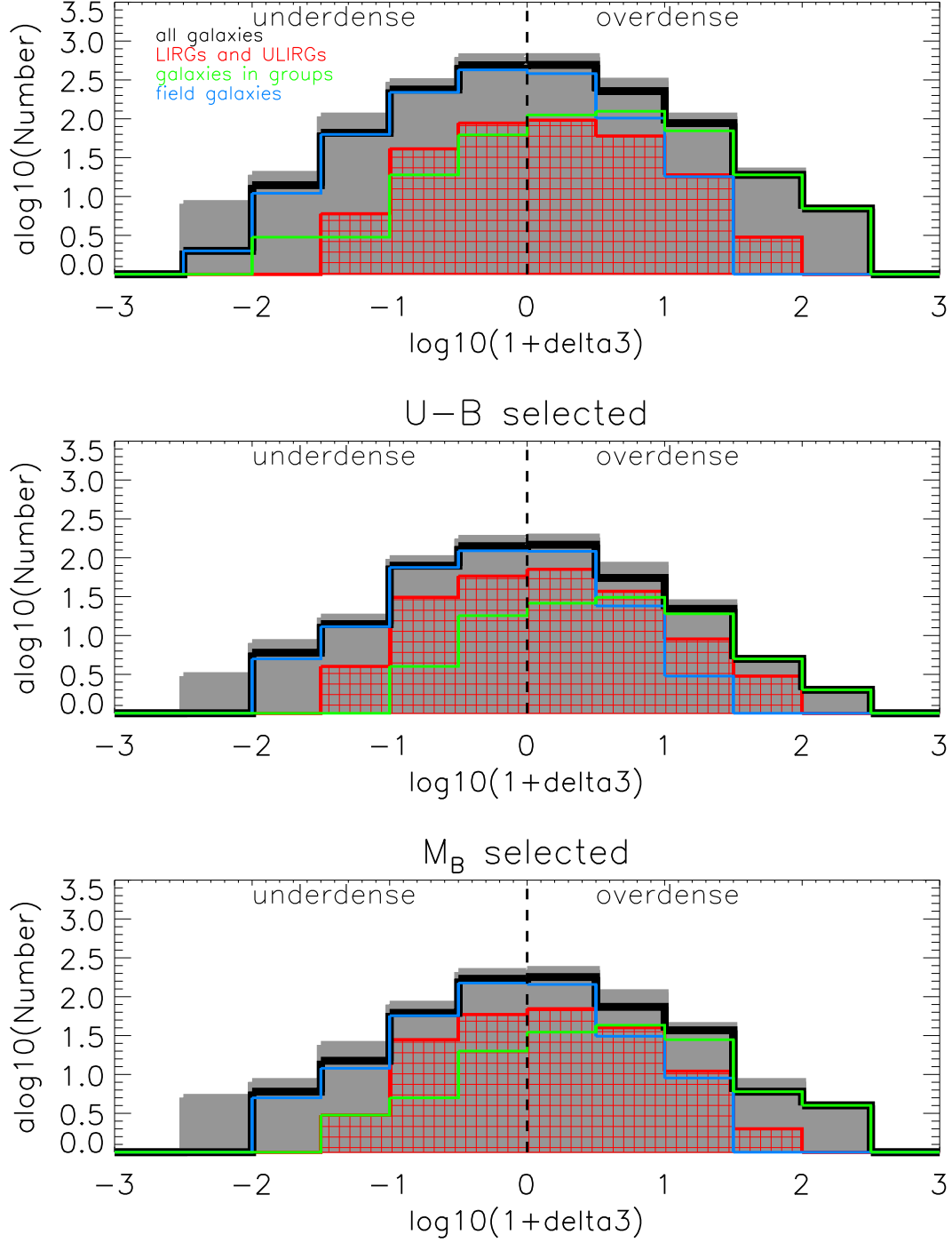


Fig. 7.— Distributions as in Figure 6 but now restricting the comparison samples to contain only non-IR galaxies.

confirmed by the fact that a majority of LIRGs and ULIRGs, i.e. 57% of them, are located in overdense regions ($D > 0$).

We have compared the local environment distribution for LIRGs and ULIRGs to that of a control sample with secure spectroscopic redshifts regardless of $24\mu\text{m}$ properties but located in the same redshift range (hereafter the “all galaxy” sample grey shaded area in Figure 6). Our findings are :

- The median LIRG and ULIRG environment is 1.2 time denser compared to the median environment of the “all galaxy” sample.
- LIRGs and ULIRGs tend to avoid very under-dense environments ($D < -1$), since only 4% of them have $D < -1$, which is 3 times less numerous than for the “all galaxy” sample. This suggests that a minimum density may be needed to trigger IR activity.
- A Kolmogorov-Smirnov (KS) test confirms that the distribution of the local environments of the “LIRG & ULIRG” and “all galaxy” samples differ significantly since the probability is $\sim 95\%$ that the distributions come from different parent populations. Once we remove the sources detected above the MIPS completeness limit belonging to the “all galaxy” sample (“all galaxy without IR” sample, hereafter), the KS test shows even stronger evidence that the local environment distribution of LIRGs and ULIRGs and of the “all galaxy” sample come from different populations. This comparison is shown in Figure 7a, where it can be seen that LIRGs and ULIRGs reside in significantly denser environments compared to other sources detected in the same redshift range.

This confirms the previous results of Cohen et al. (2000) who find that IR galaxies in the HDFN tend to belong to redshift peaks. This is also in agreement with Elbaz et al. (2007) and Cooper et al. (2007) who find that the mean SFR correlates with density at $z \sim 1$.

We have also compared the local environment of LIRGs and ULIRGs to that of sources at similar redshift and classified as group members (the “group sample”, green histogram hereafter) and field members (the “field” sample, blue histogram hereafter) in Gerke et al. (2007). The D distributions of all these samples are presented in Figure 6a. The black line indicates the D distribution of the sources that have been classified in Gerke et al. (2007)¹⁷. Our main findings are :

¹⁷They did not classify all the sources in the EGS spectroscopic redshift catalog because the EGS sampling is higher than in the three other fields studied in DEEP2. Since the group finding algorithm is optimized for a specific sampling, they re-sampled the EGS field data. It must be noticed that if the black histogram is used instead of the “all galaxy sample”, the previous results remain unchanged, which emphasizes that the two samples have very similar properties.

- The local environment of LIRGs and ULIRGs is intermediate between the “field” and “group” sources where $\langle D_{field} \rangle = -0.11$ and $\langle D_{group} \rangle = 0.52$.
- The lowest value of D for LIRGs and ULIRGs is similar to the lowest value of D for the “group sample”, while the highest is close to the “field sample” one. This implies that the LIRGs and ULIRGs tend to avoid both very under-dense and over-dense environments compared to field and group sources. These results do not change significantly if the IR sources are removed from the “all galaxy”, “field” and “group sample” as is shown in Figure 7a.

These two points will be discussed in section 7.2.

5.3. LIRGs and ULIRGs and the color-environment relation.

We discussed in the introduction how the environment of local galaxies correlates with galaxy properties such as the rest-frame colors and magnitude. Some of these relations have been extended up to $z \sim 1$ (Cooper et al., 2006). The goal of this subsection and the following one is to study the environment of LIRGs and ULIRGs in the framework of the color-environment and luminosity-environment relations.

Cooper et al. (2006) find that the fraction of red galaxies (i.e. galaxies on the red sequence, see Willmer et al., 2006) depends strongly on environment at least up to $z > 1$. We compare the mean local environment of LIRGs and ULIRGs to the one of both blue and red galaxies : In both cases, the KS test shows a significance level of 99.1% that the parent populations are different. The red galaxies exhibit a local mean environment that is ~ 1.9 times denser than the blue galaxy one; this value is slightly higher than the one given in Cooper et al. (2006) because we do not use the same samples of sources. However, the mean local environment of the red galaxies is only 1.3 times denser than the LIRG and ULIRG one. That is, the LIRGs and ULIRGs have a mean local environment that is intermediate between that of the blue and red galaxies.

We now compare the local environment of LIRGs and ULIRGs to the one of sources with similar optical colors : Figure 8a reproduces Figure 5 of Cooper et al. (2006) but restricting the sample to $0.7 \leq z \leq 1$ in the EGS field. It shows the trend of the local environment with respect to $(U-B)$ for the “all galaxies”, “field”, “group” and “LIRG & ULIRG” samples.

The thick green, blue, red¹⁸ and black lines¹⁹ represent the running median value of D as a function of $(U-B)$. The dashed lines show the 1σ error bars estimated in the same sliding box for the “LIRG & ULIRG” and “all galaxy” samples. The four samples show a strong dependence of D on $(U-B)$ and do not have identical $(U-B)$ distributions as shown in Figure 8b. While the “field”, “group” and “all galaxy” samples clearly show evidence of the color bimodality, the “LIRG & ULIRG” one exhibits a single peak in the color corresponding to “green valley”. This peak lies on the blue side of the bimodality with 84% of the LIRGs and ULIRGs on the blue side of the color-magnitude relation. The first three samples exhibit a mean color of $(U-B)=0.70^{+0.39}_{-0.20}$, $0.76^{+0.45}_{-0.23}$, $0.69^{+0.32}_{-0.18}$ respectively whereas the LIRGs and ULIRGs exhibit a mean redder color with $(U-B)=0.87^{+0.20}_{-0.17}$. As a consequence, the “field”, “group” and “all galaxy” samples studied previously are biased toward sources with bluer colors and in under-dense environments. Figure 6b presents the distribution of the “LIRG”, “group”, “field” and “all galaxy” samples restricted to the LIRG and ULIRG color range. When the “all galaxy” sample is restricted to sources with the same $(U-B)$ colors²⁰ as the LIRGs and ULIRGs, we find that the KS probability of these samples coming from the same parent population increases to $\sim 30\%$.

This result can be partly explained since all three samples are contaminated by LIRGs and ULIRGs. If we remove all IR sources from the “all galaxy”, “group” and “field” samples (see Figure 7b), the LIRGs and ULIRGs still exhibit a denser local environment than the “all galaxy sample without IR sources” since a KS test shows a probability of 3% that the “LIRG & ULIRG” and “all galaxy without IR” local environment distribution come from the same parent population. However, this color cut might not be entirely satisfactory since some residual color trends might still remain in the subsamples and could bias the result. To test this possibility, we use the “all galaxy sample” to generate ~ 100 subsamples with the same number of sources as the “LIRG and ULIRG” one and with a similar color distribution as the LIRGs and ULIRGs. Comparing the environment distribution of the LIRGs and ULIRGs with the Monte-Carlo simulations, we find that $KS = 0.41^{+0.38}_{-0.25}$ that both come from the same parent population. We also used the “all galaxy without IR” sample in a similar way and obtained $KS = 0.14^{+0.26}_{-0.10}$. These KS tests are in good agreement with the previous results.

The mean local environment of LIRGs and ULIRGs still remains denser than that of

¹⁸Due to the lack of LIRGs and ULIRGs outside the “green valley”, the mean trend and dispersion have been represented only on the $0.70 \leq (U-B) \leq 1.07$ for LIRGs and ULIRGs on Figure 8a.

¹⁹estimated using sliding boxes with $\Delta(U-B)=0.15$ for the four subsamples.

²⁰The $(U-B)$ range is $0.70 \leq (U-B) \leq 1.04$ and has been chosen to include the median $(U-B)$ with its 1σ error bar. 68% of the LIRGs and ULIRGs fall in this range.

the “field” and less dense than the “group” sample. This trend remains valid with a color selection as well as for the “all galaxy” and “all galaxy without IR” samples. Thus, LIRGs and ULIRGs are not peculiar sources; they tend to obey the same relation between over-density and rest-frame (U-B) color as is followed by other galaxies at $z \sim 1$.

However, it must be noted that even if the “all galaxy” and “all galaxy without IR sources” samples have similar M_B ($M_{B,allgalaxy} = -20.08^{+0.71}_{-0.76}$ and $M_{B,allgalaxyw/oIR} = -19.89^{+0.66}_{-0.75}$), the “LIRG & ULIRG” sample is 0.5 mag more luminous ($M_{B,LIRGsandULIRGs} = -20.60^{+0.63}_{-0.58}$). This shows that removing IR sources from the sample will bias the sample against more luminous sources with slightly different colors (see Fig.3 from Cooper et al., 2006).

5.4. LIRGs and ULIRGs and the M_B -environment relation.

Cooper et al. (2006) study the luminosity environment relation up to $z \sim 1$. They show that the luminosity is a function of environment for both blue and red galaxies at $z \sim 1$ (see their Figure 9). They find that bright blue galaxies are in over-dense regions, contrasting with the local universe where no correlation has been identified between luminosity and over-density for blue galaxies. Cooper et al. (2007) interpret this relation as evidence for the different relation between SFR and environment at $z \sim 1$. Figure 9a shows the dependence of the local environment with respect to M_B for the “all galaxies”, “field”, “group” and “LIRG & ULIRG” samples, where it is seen that bright sources tend to be found in over-dense environments. However, as is shown in Figure 9b, the LIRGs and ULIRGs have a median of $M_B = -20.64^{+0.71}_{-0.53}$, which is roughly one magnitude brighter than the mean luminosity of other sources located in the same redshift range. LIRGs and ULIRGs tend to occupy a very similar environment as the bright sources in the “all galaxy” sample.

To quantify this result, we restricted all the samples to sources with similar M_B^{21} as the LIRGs and ULIRGs. The results are presented in Figure 6c (and 7c for the sample where the IR sources have been removed). The first point is that the difference between the “LIRG and ULIRG” and “all galaxy” or “all galaxy - IR” local environment distributions

²¹-21.18 $\leq M_B \leq$ -19.93 (which contains 68% of the LIRGs and ULIRGs, including the median value and 1σ error bar.)

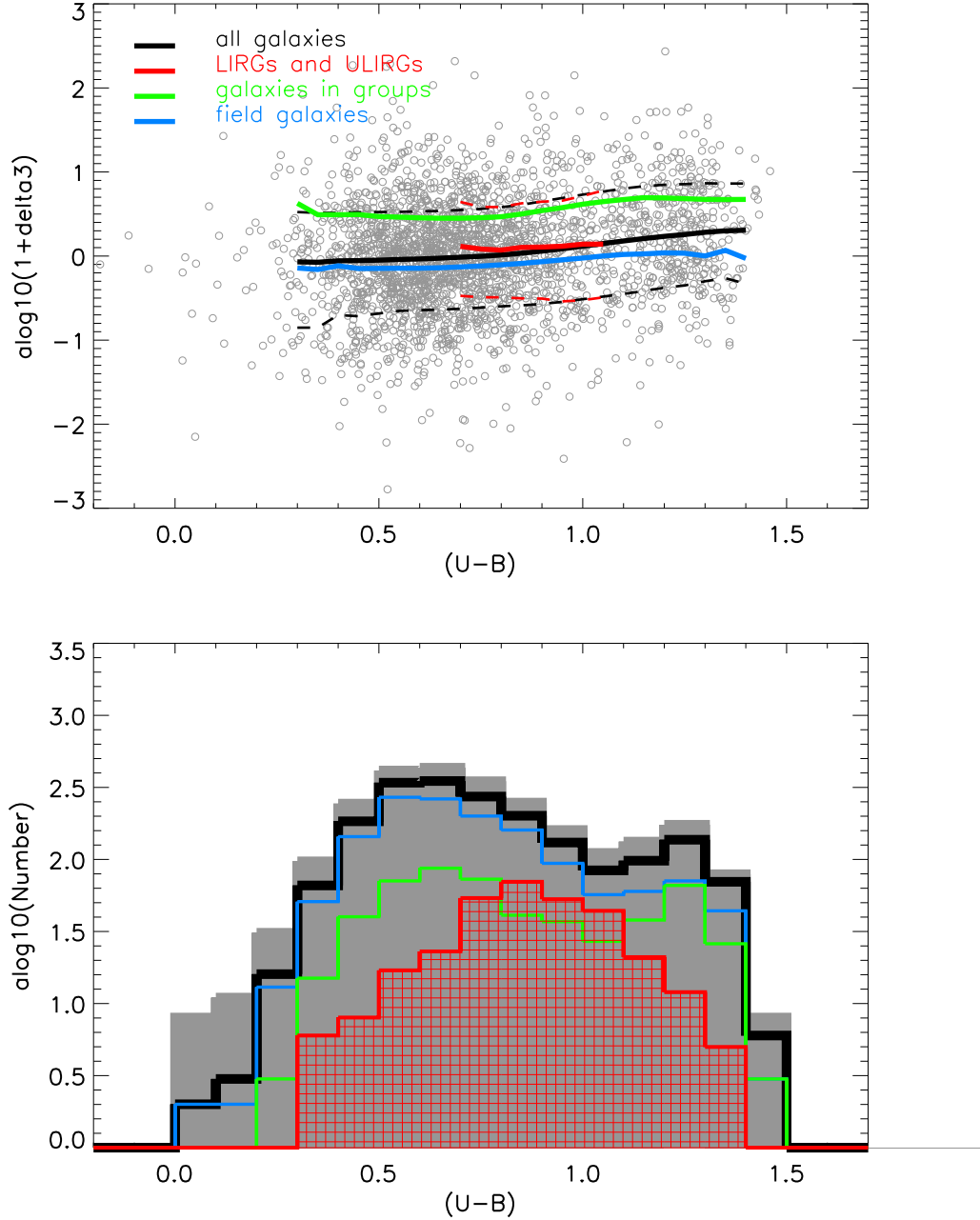


Fig. 8.— **Top** : Environment as a function of the $(U-B)$ color. The black, red, green and blue lines show the mean evolution of the “all galaxy”, “LIRG and ULIRG”, “group” and “field” samples. They have been computed in sliding boxes with $\Delta(U-B)=0.15$ for the four subsamples. The dashed lines show the 1σ error bars estimated in a sliding box with similar size. Due to the lack of LIRGs and ULIRGs outside the “green valley”, the mean trends have been represented for $0.70 \leq (U-B) \leq 1.07$ which is the color range of the 68% of the LIRGs and ULIRGs. The mean local environment of LIRGs and ULIRGs is very similar to the one of sources with similar colors, but still remains denser than that of the “field” and less dense than the “group” sample. **Bottom** : Comparison of the histograms of $(U-B)$ colors for all the “all galaxy”, “LIRG and ULIRG”, “group” and “field” samples.

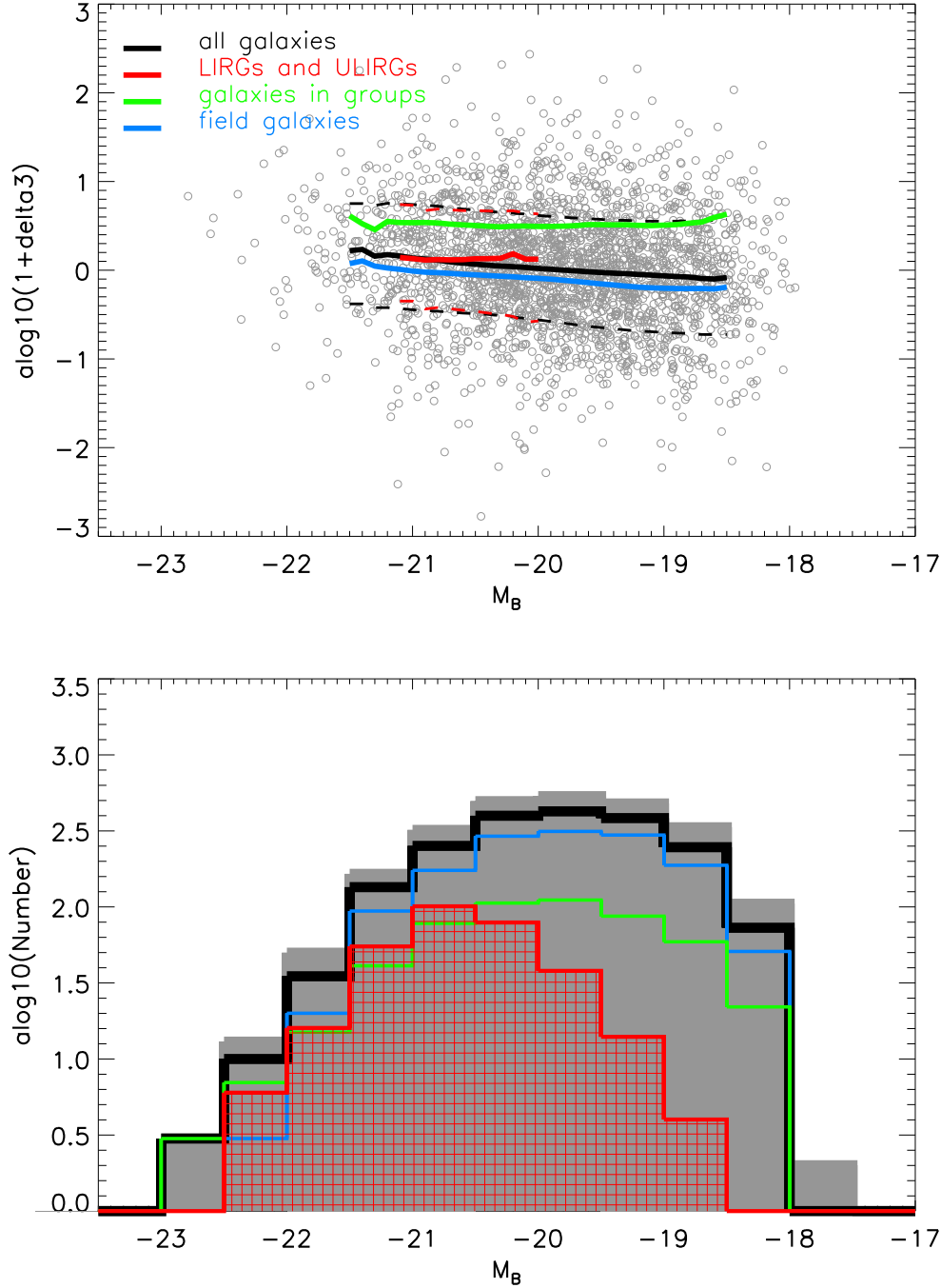


Fig. 9.— **Top :** Environment as a function of M_B . The black, red, green and blue lines show the mean trend of the “all galaxy”, “LIRG”, “group” and “field” samples. They have been computed in sliding boxes with $\Delta(M)_B=0.3$ for the four subsamples. The dashed lines show the 1σ error bars estimated in a sliding box with similar size. The mean local environment of LIRGs and ULIRGs is very similar to the one of sources with similar optical luminosity, but still remains denser than that of the “field” and less dense than the “group” sample. **Bottom :** Comparison of the histograms of the M_B colors for the “all galaxy”, “LIRG and ULIRG”, “group” and “field” samples.

is no longer significant since the KS tests give the probability that the “LIRG and ULIRG” local environment distribution comes from the “all galaxy” or “all galaxy without IR” one is within 1σ . However, this magnitude cut might not be entirely satisfactory since some residual magnitude trends might remain in the subsamples and could bias the result. We have then used the “all galaxy” sample to generate ~ 100 subsamples with the same number of sources as the “LIRG and ULIRG” one and that reproduce the magnitude distribution of LIRGs and ULIRGs. We obtain a KS probability of $0.73^{+0.21}_{-0.26}$ that the “LIRG and ULIRG” local environment distribution and the Monte-Carlo generated ones come from a similar parent population, so there are no longer significant differences. We also use the “all galaxy sample without IR sources” in a similar way and obtain $\text{KS}=0.60^{+0.25}_{-0.18}$. As a consequence, the trend that LIRGs and ULIRGs are in denser environments is substantially weakened when considering sources with similar luminosities. Thus, the LIRGs and ULIRGs tend to have similar local environments as sources located in the same luminosity range. This shows that LIRGs and ULIRGs do not tend to be peculiar objects in the local over-density - M_B relation.

The second result is that the local environment of LIRGs and ULIRGs still remains significantly denser than that of the “field” and less dense than the “group” samples. This trend remains valid with a magnitude selection as well as for “all galaxy” and “all galaxy without IR” samples.

5.5. LIRGs and ULIRGs and the color - magnitude relation.

Although we had previously found that LIRGs and ULIRGs lie in denser mean environments than all the galaxies in a similar redshift range, in the two previous subsections, we saw that this trend is weaker when comparing to galaxies with similar color or magnitude. However, within color- or magnitude-selected samples, the mean magnitude - color behavior of LIRGs and ULIRGs differs from that of the other galaxies. This can be seen in Figure 10, which presents the (U-B) color as a function of M_B ; the black open circles represent all the galaxies in a similar redshift range as the LIRGs and ULIRGs while the red plain ones are the LIRGs and ULIRGs. The big red dot shows the median magnitude and color value for LIRGs and ULIRGs with a 1σ error bar. For the given mean “LIRG and ULIRG” luminosity, LIRGs and ULIRGs tend to have bluer colors. This can also be interpreted that for a given mean “LIRG and ULIRG” color, LIRGs and ULIRGs tend to be bright in the optical.

We have therefore tested our results against a color - magnitude selection to compare very similar optical sources. We used the “all galaxy sample” to generate ~ 100 Monte Carlo subsamples with the same number of sources as the “LIRG” sample and the same color and

magnitude distribution. We obtained $KS=0.90^{+0.06}_{-0.23}$ that the two distributions come from the same population. We obtained $KS=0.55^{+0.27}_{-0.22}$ for the “all galaxy without IR sample”. LIRGs and ULIRGs tend to have a very similar mean environment as sources with similar color and magnitude disregarding their IR activity. These results are very close to the ones obtained for luminosity selected samples as discussed in the previous subsection.

We also find that the local environment of LIRGs and ULIRGs still remains significantly denser than that of the “field” and less dense than the “group” samples. This trend remains valid with a color-magnitude selection as well as for “all galaxy” and “all galaxy without IR” samples.

5.6. Studying LIRGs and ULIRGs in mass selected samples.

It is difficult to interpret these results because they rely on color and luminosity, which might not be the best descriptors for LIRGs and ULIRGs when compared to non-IR sources. LIRGs and ULIRGs are intrinsically brighter mainly because they are forming young stars. Both the R-band selection of DEEP2 (rest-frame 3400 Å) and the comparison at fixed M_B will combine smaller blue galaxies with larger red galaxies. Therefore, we now test the dependence of our results against a mass selection.

For the portion of the EGS imaged with J and Ks at Palomar, Bundy et al. (2006) estimated stellar masses using BRIJK photometry and synthetic SEDs from Bruzual & Charlot (2003), which span a large range of star formation history and metallicities. To extend the stellar mass estimates to the whole EGS, we use the mean relation of Lin et al. (2007) derived from the Bell & de Jong (2001) prescription. We find no systematic differences between masses estimated from Bundy et al. (2006) and Lin et al. (2007) for LIRGs and ULIRGs.

We restricted all samples to the $2-7 \times 10^{10} M_\odot$ range, which includes 68% of the LIRG and ULIRG mass range. The results are presented in Figure 11a and b for the normal samples and for the samples where IR sources have been removed. We generated 100 Monte Carlo subsamples for the “all galaxy sample” and “all galaxy without IR sample” to match the mass distribution of LIRGs and ULIRGs. We obtain a KS probability of $0.80^{+0.10}_{-0.26}$ and $0.63^{+0.22}_{-0.22}$ respectively that the LIRG and ULIRG local environment distribution and the generated ones come from a similar parent population. This behavior is very similar to that we find for the magnitude or magnitude - color selection. This is the consequence of the masses having been estimated as a function of both M_B and U-B; however, the masses depend on M_B to first order while the color correction is a second order effect (Bell et al.,

2005, Lin et al., 2007).

The local environment of LIRGs and ULIRGs still remains significantly denser than that of the “field” and less dense than the “group” samples. This trend remains valid with a mass selection as well as for the “all galaxy” and “all galaxy without IR” samples .

6. What fraction of LIRGs and ULIRGs are classified as group members ?

In contrast to the local clusters (Fadda et al., 2000), LIRGs and ULIRGs have been found in dense environments such as dense clusters and can be found in excess in some of them when compared to field sources at $0.5 < z < 0.9$, (Geach et al., 2006, Marcillac et al., 2007, Bai et al., 2007). However the number of LIRGs and ULIRGs in very dense environments (clusters or outskirts of clusters) is small and not representative of the mean environment of the whole population. We now know that IR galaxies tend to have a mean local environment that is significantly denser than non group member sources and significantly less dense than “group” members; this statement has been tested against rest-frame colors and luminosity and mass. However we would like to estimate the fraction of sources that are group members.

Gerke et al. (2005) show that field sources represent roughly 67% of the DEEP2 survey. They also represent roughly 73% of the galaxies in the EGS. The remaining sources belong to groups. We have used the “group member” indicator as a way to test in an independent way the environment of LIRGs and ULIRGs.

Gerke et al. (2005), did not classify all sources in the EGS spectroscopic redshift catalog because the EGS sampling is slightly higher than in the three other fields studied in DEEP2. Since the group finding algorithm is optimized for a specific sampling, they re-sampled the EGS field data. Therefore, in this section we have restricted the four samples defined in section 5 to the subsamples of sources that have been analysed using the group-finding algorithm. In the “all galaxy” sample, 27% of the sources are group members. This value decreases to 25% if the MIPS sources are removed from the sample. In comparison, 33% of the LIRGs and ULIRGs belong to groups. We performed a Monte Carlo simulation to test if this difference is significant. We used the “all galaxy” sample to generate ~ 10000 subsamples with the same number of sources as the “LIRG and ULIRG” one and studied the distribution of the fraction of group members. Only 1.1% the “all galaxy” sample have a ratio as high as the MIPS sample, which suggests that this difference is significant. The difference is even higher if we make the Monte Carlo simulation using the sample of “all field without IR ”. This confirms that the IR sources lie more often in groups than the non-IR sources and agrees with local over-density estimator findings.

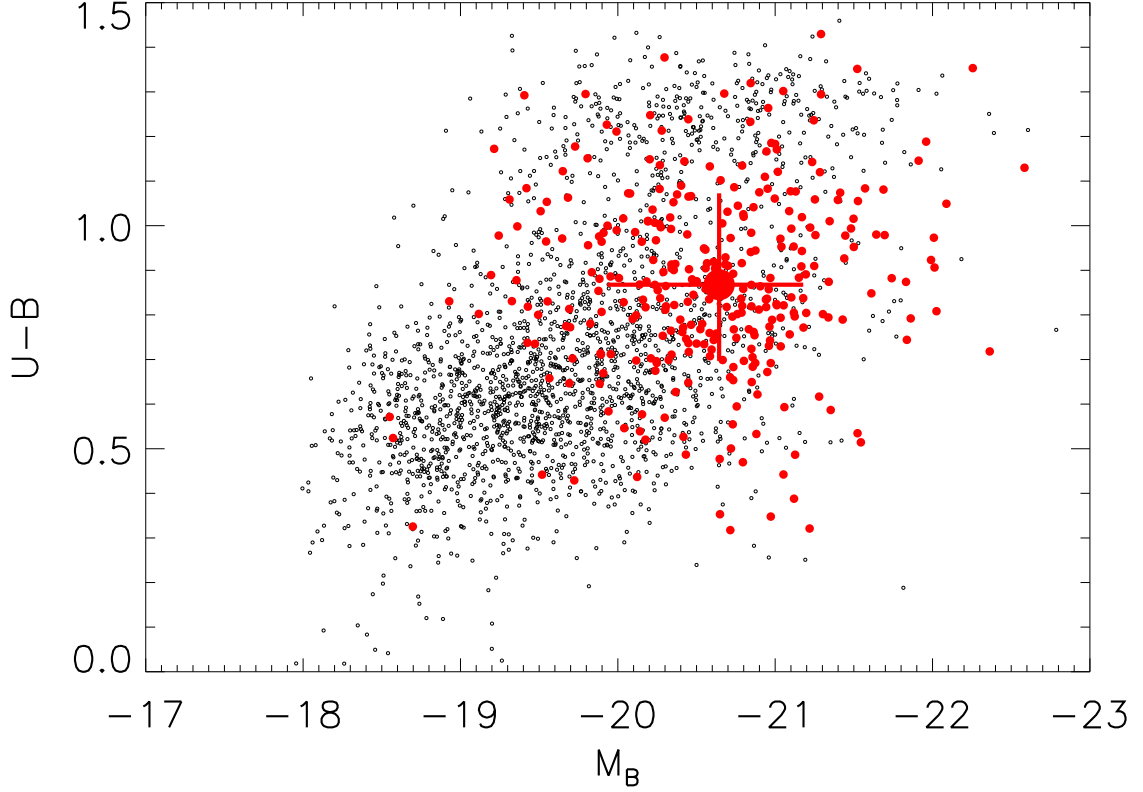


Fig. 10.— $(U-B)$ color as a function of M_B . The black open circles represent galaxies in a similar redshift range as the LIRGs and ULIRGs while the red plain ones are the LIRGs and ULIRGs. The big red dot is associated with the median magnitude and color value for LIRGs and ULIRGs with a 1σ error bar. For the given mean “LIRG and ULIRG” luminosity, LIRGs and ULIRGs tend to have bluer colors than sources located in a similar redshift range. This can also be interpreted that for a given mean “LIRG and ULIRG” color, LIRGs and ULIRGs tend to be optically brighter. [*See the electronic edition of the Journal for a color version of this figure.*]

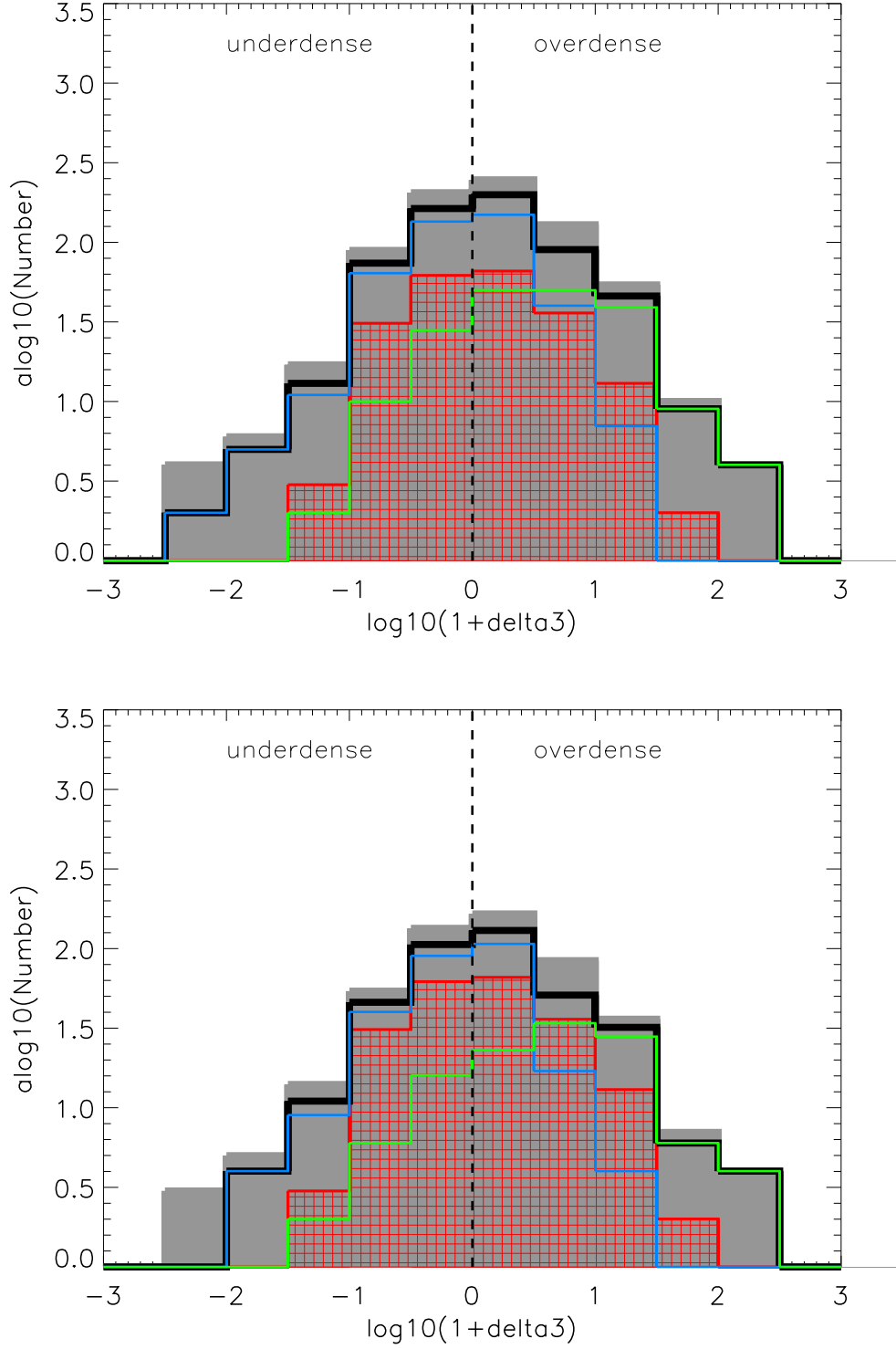


Fig. 11.— Distribution of the local galaxy environment for the mass selected sample. **Top :** Sample with IR galaxies (like in Figure 6). **Bottom :** Sample with all sources not detected at $24 \mu\text{m}$ (like in Fig 7).

However, as seen in section 4.3, the results concerning the local over-density estimators are strongly affected if we compare the “LIRG and ULIRG” environment to that of sources selected in color, luminosity or mass bins. We have therefore studied the fraction of *group* members in color, luminosity and mass selected samples to test this issue. The results are presented in Table 4. We performed a Monte Carlo simulation to estimate the validity of each result. Although the fraction of LIRGs and ULIRGs that are group members tends to be higher when compared to sources with similar colors and luminosities, the Monte Carlo simulation shows that the difference is less significant than previously. All differences vanish when studying the mass selected samples. This confirms in an independent way the results found in the previous section. LIRGs and ULIRGs are more often found in groups compared to the general population of galaxies located in the same redshift range. However, this difference is weakened or vanishes when they are compared to a sample of galaxies with similar color, luminosity or mass.

7. Influence of the environment on LIRG and ULIRG activity at $z \sim 1$.

7.1. Contribution of LIRGs and ULIRGs to SFR(IR) at $z \sim 1$ as a function of environment

In this section we examine the contribution to the total SFR of IR galaxies in different environments. We saw in section 6 that LIRGs and ULIRGs tend to avoid very under-dense environments, but otherwise are found in a large diversity of environments at $z \sim 1$, ranging from clusters (Geach et al., 2007, Marcillac et al., 2007), to groups or less dense structures. LIRGs and ULIRGs have been shown to play a significant role in galaxy evolution at $z \sim 1$: Le Floc’h et al. (2005) show that the space density of LIRGs and ULIRGs is more than 100 times their density in the local universe. At $z \sim 0.7$, they have the same contribution to the SFR as the star forming galaxies, and they dominate the SFR at higher redshift. A negligible fraction of LIRGs and ULIRGs belong to clusters or bigger bound structures; one reason is that these structures have a low number density at $z \sim 1$. Therefore we have neglected their contribution. In Section 6, we show that $\sim 30\%$ of LIRGs and ULIRGs are associated with groups in the EGS and this number weakly depends on color, luminosity and mass selection. At $z \sim 1$, LIRGs and ULIRGs are responsible for $\sim 70\%$ of the comoving energy density (Le Floc’h et al. 2005); The contribution of LIRGs and ULIRGs that are “group members” can be estimated to be $0.7 \times 0.3 \sim 20\%$, while the contribution from “non group members” is $\sim 50\%$. This implies that 20 % of the sources responsible for the IR star formation rate density and comoving energy density belong to groups in DEEP2 and are hosted by a dark matter halo with a lower limit mass of $6 \times 10^{12} M_{\odot} h^{-1}$.

7.2. Physical environment of IR-galaxies.

Here, we further characterize the environment of IR galaxies. We saw that LIRGs and ULIRGs tend to be in denser environments when compared to all $R \leq 24.1$ galaxies and have an environment that is intermediate between blue and red galaxies; but this difference vanishes when their environment is compared to that of sources with similar color, luminosity or mass. Thus, LIRGs and ULIRGs are not outliers of the color-environment relations at $z \sim 1$, since they have a similar environment as the other “green valley” galaxies. They also follow the luminosity-environment relations at $z \sim 1$. LIRGs and ULIRGs always tend to be in a denser environment than “field” galaxies and less dense than “group” galaxies regardless of color, magnitude or mass selection.

To go further, Coil et al. (2007) take advantage of the whole DEEP2 Galaxy Redshift Survey data to study the clustering properties of the “green valley” galaxies and show that they exhibit an intermediate clustering amplitude to red and blue galaxies. On large scales, they tend to have a clustering amplitude similar to that of red galaxies where at small scales, the amplitude is closer to that of blue galaxies. “Green” galaxies are also found to have intermediate-strength “fingers-of-god” and have comparable kinematics to blue galaxies. They interpret these results as showing the “green valley” galaxies are in the same dense regions as the red galaxies but are less likely than red galaxies to lie at the cores of the overdensities. They suggest that “green valley” galaxies could reside on the outskirts of the same halos that red galaxies occupy. This interpretation is in good agreement with our results. It also agrees with the result of Cohen et al. (1999) and Gilli et al. (2007). Cohen et al. found that the MIR sources appear to be more clustered than the optical sources with $\sim 90\%$ of them lying within the statistically complete sample of redshift peaks. Gilli et al. found that LIRGs and ULIRGs in GOODS tend to be more clustered ($r_0 = 5.1 \pm 0.8 \text{ h}^{-1} \text{ Mpc}$) than the optically selected sources. Furthermore, this behavior is in agreement with the overall correlation between environment and SFR found at $z \sim 1$ (Cooper et al., 2007, Elbaz et al., 2007).

It must be noted that very dense structure such as clusters or big groups have not been identified in EGS or GOODS-N and GOODS-S. Interestingly, distant ($z \sim 0.8$) clusters show that LIRGs and ULIRGs are mainly found in the cluster outskirts and tend to have similar properties as the LIRGs and ULIRGs identified in the DEEP field surveys (Marcillac et al., 2007, Bai et al., 2007). This result appears to conflict with Elbaz et al. (2007), who found a structure at $z = 1.016$ where the most vigorously star-forming galaxies are at the center of the groups. However, the results can be reconciled if the structure identified at $z = 1.016$ is at an earlier stage of forming a cluster.

The tendency of LIRGs and ULIRGs to belong to the outskirts of structures such as

groups may suggest mechanisms responsible for the IR activity. Due to the incompleteness of the EGS spectroscopic redshifts, we can not exclude major mergers and strong galaxy–galaxy interactions from being an important mechanism to trigger IR activity. However, morphological studies have shown that mergers are not the only mechanism triggering LIRGs and ULIRGs at these redshifts (e.g., Lotz et al. 2006). If LIRGs and ULIRGs mainly belong to the outskirts of groups, galaxy-galaxy interaction such as minor mergers and pair interactions can play a role. The photometric and spectroscopic data used here are limited to $R=24.1$, which places a strong constraint on the upper mass limit of a companion that we might detect that could be responsible for triggering IR-activity. To estimate it, we have selected a sample of sources at $R\sim 24$ at $0.7 < z < 1$; they tend to have $\log(M) \sim 10.0^{+0.3}_{-0.1}$ for red galaxies and $\log(M) \sim 9.3^{+0.3}_{-0.3}$ for blue ones. This mass range prevents us from studying minor mergers around IR galaxies, especially if the satellite is on the red side of the bimodality. Thus, minor mergers and interactions with small satellites might be partly responsible for IR-activity. This is in agreement with morphology studies at $z \sim 1$, which suggest that among the LIRGs classified as “isolated spiral galaxies”, some show signs of asymmetry and disturbance that are too weak to be associated with a major merger (Shi et al. 2006).

Weak interactions such as widely separated pairs can be another mechanism triggering IR activity. Lin et al.(2007) study the mid-IR properties and star formation of galaxy pairs and find a mid-IR enhancement for ULIRGs in pairs separated by less than a few tens of kpc. In addition, a smoother/weaker interaction between two galaxies with a larger separation could account for some enhancement of the star-formation activity. If the separation is large enough, the galaxies will not be classified as “close pair” sources but as two isolated galaxies that do not belong to bound structures. Thus, we cannot rule out from this study that the environment might play a role in IR activity through interactions such as minor mergers or by widely separated pairs.

Do such interactions play a stronger role for IR galaxies than for sources of similar masses or luminosities? Or does the high IR luminosity have some “duty cycle” and all objects in overdense environments go through a LIRG or ULIRG phase (in which case, one can wonder if the environment is responsible for the IR activity, or just correlated with it)? It is also possible that the environment plays a very minor role in IR-activity, and that internal causes are responsible.

8. Conclusion

Using a combination of MIPS $24\mu\text{m}$ data with the multi-wavelength data available in the extended Groth strip (EGS), we investigate the role that the environment plays in the

LIRG and ULIRG phenomena. Two environment indicators were used : the first one is a local environment estimator, the second is based on an algorithm that identifies groups and bound structures. These estimators are independent. We concentrate on IR-galaxies located at $0.7 < z < 1$, where they dominate the IR luminosity function and star formation rate.

Our results are as follows :

- There is no trend between L_{IR} and the local environment of LIRGs, showing that the environment is not gradually quenching or triggering the IR – activity at $z \sim 1$.
ULIRGs tend to be in over-dense environments. However, they are also optically brighter than LIRGs and tend to have an environment comparable to sources with similar optical luminosity.
- We find that LIRGs and ULIRGs have a mean local environment that is intermediate between those of blue and red galaxies.
They also tend to avoid very underdense ($D < -1$) environments.
LIRGs and ULIRGs are found in 1.2 times denser mean local environments than that of other DEEP2 galaxies at similar redshift.
- We find that the LIRG and ULIRG local environment differences decrease when compared to sources with similar rest frame (U-B) color and vanish when compared to sources with similar mass, M_B or M_B -color distribution. Thus, LIRGs have similar environment properties as “green valley” galaxies; LIRGs and ULIRGs are not outliers of the color-environment and magnitude-environment relations at $z \sim 1$.
- The local environment of LIRGs and ULIRGs still remains significantly denser than that of the “field” and less dense than the “group” samples. This trend remains valid with a magnitude, color, color magnitude or mass selection selection. These results are comparable to the picture given in Coil et al. (2007) where “green valley” galaxies could reside on the outskirts of the same halos that red galaxies occupy.
- We find that about 30% of LIRGs belong to groups with a minimum dark matter halo mass of $6 \times 10^{12} M_{\odot} h^{-1}$; They constitute 20 % of the sources responsible for the IR star formation rate density and comoving energy density at $z \sim 1$.

This work is based on observations made with the *Spitzer* Space Telescope, which is operated by the Jet Propulsion Laboratory, California Institute of Technology under a contract with NASA (contract number #1407). Support for this work was provided by NASA through an award issued by JPL/Caltech (contract number #1255094).

This paper makes use of DEEP2 and EGS data. Funding for the DEEP2 survey has been provided by NSF grant AST05-07428 and AST05-07483. Some of the data presented here were obtained at the W.M. Keck Observatory, which is operated as a scientific partnership among the California Institute of Technology, the University of California and the National Aeronautics and Space Administration. The Observatory was made possible by the generous financial support of the W.M. Keck Foundation. The DEEP2 team and Keck Observatory acknowledge the very significant cultural role and reverence that the summit of Mauna Kea has always had within the indigenous Hawaiian community and appreciate the opportunity to conduct observations from this mountain.

This paper makes use of photometric redshifts produced jointly by Terapix and the VVDS teams, and the CENCOS interface (<http://cencosw.oamp.fr>) was used for data retrieval and analyses. This work is based on observations made with the *Spitzer* Space Telescope, which is operated by the Jet Propulsion Laboratory, California Institute of Technology under a contract with NASA (contract number #1407). Support for this work was provided by NASA through an award issued by JPL/Caltech (contract number #1255094).

The authors would like to thank the anonymous referee for helpful comments. ESL acknowledges the support of STFC. M.C.C. acknowledges support provided by the *Spitzer Space Telescope* Fellowship Program, through a NASA grant administered by the Jet Propulsion Laboratory at the California Institute of Technology.

REFERENCES

- Alonso-Herrero, A. 2006, ArXiv Astrophysics e-prints
- Alonso-Herrero, A. et al. 2006, ApJ, 640, 167
- Bai, L. et al. 2007, ApJ, 664, 181
- Balogh, M. et al. 2004, MNRAS, 348, 1355
- Balogh, M. L., Morris, S. L., Yee, H. K. C., Carlberg, R. G., & Ellingson, E. 1999, ApJ, 527, 54
- Barmby, P. et al. 2006, ApJ, 642, 126
- Beckwith, S. V. W. 2005, VizieR Online Data Catalog, 2258, 0
- Bell, E. F. 2002, ApJ, 581, 1013
- Bell, E. F., & de Jong, R. S. 2001, ApJ, 550, 212

- Bell, E. F., McIntosh, D. H., Katz, N., & Weinberg, M. D. 2003, *ApJS*, 149, 289
- Bell, E. F. et al. 2005, *ApJ*, 625, 23
- Blanton, M. R. et al. 2003, *ApJ*, 594, 186
- Bridge, C. R. et al. 2007, *ApJ*, 659, 931
- Bruzual, G., & Charlot, S. 2003, *MNRAS*, 344, 1000
- Bundy, K. et al. 2006, *ApJ*, 651, 120
- Caputi, K. I. et al. 2007, *ApJ*, 660, 97
- Chary, R., & Elbaz, D. 2001, *ApJ*, 556, 562
- Cohen, J. G., Hogg, D. W., Blandford, R., Cowie, L. L., Hu, E., Songaila, A., Shopbell, P., & Richberg, K. 2000, *ApJ*, 538, 29
- Coil, A. L. et al. 2007, *ArXiv e-prints*, 708
- Coil, A. L., Newman, J. A., Kaiser, N., Davis, M., Ma, C.-P., Kocevski, D. D., & Koo, D. C. 2004, *ApJ*, 617, 765
- Colless, M. et al. 2001, *MNRAS*, 328, 1039
- Conselice, C. J., Bershad, M. A., Dickinson, M., & Papovich, C. 2003a, *AJ*, 126, 1183
- Conselice, C. J., Chapman, S. C., & Windhorst, R. A. 2003b, *ApJ*, 596, L5
- Cooper, M. C. et al. 2006, *MNRAS*, 370, 198
- Cooper, M. C., Newman, J. A., Madgwick, D. S., Gerke, B. F., Yan, R., & Davis, M. 2005, *ApJ*, 634, 833
- Cooper, M. C. et al. 2007, *ArXiv e-prints*, 706
- Dale, D. A., & Helou, G. 2002, *ApJ*, 576, 159
- Davis, M. et al. 2003, in Presented at the Society of Photo-Optical Instrumentation Engineers (SPIE) Conference, Vol. 4834, Discoveries and Research Prospects from 6- to 10-Meter-Class Telescopes II. Edited by Guhathakurta, Puragra. Proceedings of the SPIE, Volume 4834, pp. 161-172 (2003)., ed. P. Guhathakurta, 161–172
- Davis, M., & Geller, M. J. 1976, *ApJ*, 208, 13

- Davis, M., Gerke, B. F., Newman, J. A., & the Deep2 Team. 2005, in *Astronomical Society of the Pacific Conference Series*, Vol. 339, *Observing Dark Energy*, ed. S. C. Wolff & T. R. Lauer, 128–+
- Davis, M. et al. 2007, *ApJ*, 660, L1
- Desert, F.-X., Boulanger, F., & Puget, J. L. 1990, *A&A*, 237, 215
- Donley, J. L., Rieke, G. H., Pérez-González, P. G., Rigby, J. R., & Alonso-Herrero, A. 2007, *ApJ*, 660, 167
- Dressler, A. 1980, *ApJ*, 236, 351
- Einasto, J., Tago, E., Einasto, M., Saar, E., Suhhonenko, I., Heinämäki, P., Hütsi, G., & Tucker, D. L. 2005, *A&A*, 439, 45
- Elbaz, D. et al. 2007, *A&A*, 468, 33
- Faber, S. M. et al. 2003, in *Presented at the Society of Photo-Optical Instrumentation Engineers (SPIE) Conference*, Vol. 4841, *Instrument Design and Performance for Optical/Infrared Ground-based Telescopes*. Edited by Iye, Masanori; Moorwood, Alan F. M. *Proceedings of the SPIE*, Volume 4841, pp. 1657-1669 (2003)., ed. M. Iye & A. F. M. Moorwood, 1657–1669
- Fadda, D., Elbaz, D., Duc, P.-A., Flores, H., Franceschini, A., Cesarsky, C. J., & Moorwood, A. F. M. 2000, *A&A*, 361, 827
- Fazio, G. G. et al. 2004, *ApJS*, 154, 10
- Fisher, K. B., Davis, M., Strauss, M. A., Yahil, A., & Huchra, J. 1994, *MNRAS*, 266, 50
- Freyer, D. T. et al. 2006, *AJ*, 131, 250
- Geach, J. E., Smail, I., Chapman, S. C., Alexander, D. M., Blain, A. W., Stott, J. P., & Ivison, R. J. 2007, *ApJ*, 655, L9
- Geach, J. E. et al. 2006, *ApJ*, 649, 661
- Gerke, B. F. et al. 2005, *ApJ*, 625, 6
- . 2007, *MNRAS*, 376, 1425
- Gómez, P. L. et al. 2003, *ApJ*, 584, 210
- Gonzalez-Solares, E. A. et al. 2004, *MNRAS*, 352, 44

- Gordon, K. D. et al. 2005, *PASP*, 117, 503
- Hammer, F., Flores, H., Elbaz, D., Zheng, X. Z., Liang, Y. C., & Cesarsky, C. 2005, *A&A*, 430, 115
- Houck, J. R. et al. 2005, *ApJ*, 622, L105
- Ilbert, O. et al. 2006a, *A&A*, 457, 841
- . 2006b, *ArXiv Astrophysics e-prints*
- Ishida, C. M. 2004, PhD thesis, AA(UNIVERSITY OF HAWAII)
- Kennicutt, Jr., R. C. 1998, *ApJ*, 498, 541
- La Franca, F. et al. 2004, *AJ*, 127, 3075
- Le Fèvre, O. et al. 2004, *A&A*, 428, 1043
- Le Floc’h, E. et al. 2005, *ApJ*, 632, 169
- . 2004, *ApJS*, 154, 170
- Liang, Y. C., Hammer, F., Flores, H., Elbaz, D., Marcillac, D., & Cesarsky, C. J. 2004, *A&A*, 423, 867
- Lin, L. et al. 2007, *ApJ*, 660, L51
- Lotz, J. M. et al. 2006, *ArXiv Astrophysics e-prints*
- Marcillac, D., Elbaz, D., Chary, R. R., Dickinson, M., Galiano, F., & Morrison, G. 2006, *A&A*, 451, 57
- Marcillac, D., Rigby, J. R., Rieke, G. H., & Kelly, D. M. 2007, *ApJ*, 654, 825
- Marinoni, C., Davis, M., Newman, J. A., & Coil, A. L. 2002, *ApJ*, 580, 122
- Melbourne, J., Koo, D. C., & Le Floc’h, E. 2005, *ApJ*, 632, L65
- Mirabel, I. F. et al. 1998, *A&A*, 333, L1
- Nandra, K. et al. 2005, *MNRAS*, 356, 568
- Norberg, P. et al. 2001, *MNRAS*, 328, 64
- Oemler, A. J. 1974, *ApJ*, 194, 1

- Oliver, S., & Pozzi, F. 2005, *Space Science Reviews*, 119, 411
- Oliver, S. et al. 2000, *MNRAS*, 316, 749
- Owers, M., Blake, C., Couch, W., Pracy, M., & Bekki, K. 2007, *ArXiv e-prints*, 707
- Papovich, C. et al. 2004, *ApJS*, 154, 70
- . 2007, *ArXiv e-prints*, 706
- Park, C., Choi, Y.-Y., Vogeley, M. S., Gott, J. R. I., & Blanton, M. R. 2007, *ApJ*, 658, 898
- Pérez-González, P. G. et al. 2005, *ApJ*, 630, 82
- Piccinotti, G., Mushotzky, R. F., Boldt, E. A., Holt, S. S., Marshall, F. E., Serlemitsos, P. J., & Shafer, R. A. 1982, *ApJ*, 253, 485
- Postman, M., & Geller, M. J. 1984, *ApJ*, 281, 95
- Puget, J. L., & Leger, A. 1989, *ARA&A*, 27, 161
- Ranalli, P., Comastri, A., & Setti, G. 2003, *A&A*, 399, 39
- Rieke, G. H. et al. 2004, *ApJS*, 154, 25
- Rigby, J. R. et al. 2004, *ApJS*, 154, 160
- Rigopoulou, D., Kunze, D., Lutz, D., Genzel, R., & Moorwood, A. F. M. 2002, *A&A*, 389, 374
- Rowan-Robinson, M. et al. 2005, *AJ*, 129, 1183
- . 2004, *MNRAS*, 351, 1290
- Sanders, D. B., & Mirabel, I. F. 1996, *ARA&A*, 34, 749
- Sanders, D. B., Soifer, B. T., Elias, J. H., Neugebauer, G., & Matthews, K. 1988, *ApJ*, 328, L35
- Saunders, W., Rowan-Robinson, M., & Lawrence, A. 1992, *MNRAS*, 258, 134
- Scoville, N. et al. 2006, *ArXiv Astrophysics e-prints*
- Sheth, R. K., & Tormen, G. 1999, *MNRAS*, 308, 119

- Shi, Y., Rieke, G. H., Papovich, C., Pérez-González, P. G., & Le Floch, E. 2006, *ApJ*, 645, 199
- Simpson, C., & Eisenhardt, P. 1999, *PASP*, 111, 691
- Soifer, B. T., & Neugebauer, G. 1991, *AJ*, 101, 354
- Soifer, B. T., Sanders, D. B., Madore, B. F., Neugebauer, G., Danielson, G. E., Elias, J. H., Lonsdale, C. J., & Rice, W. L. 1987, *ApJ*, 320, 238
- Stetson, P. B. 1987, *PASP*, 99, 191
- Tanaka, M., Goto, T., Okamura, S., Shimasaku, K., & Brinkmann, J. 2004, *AJ*, 128, 2677
- Wang, J. L., Xia, X. Y., Mao, S., Cao, C., Wu, H., & Deng, Z. G. 2006, *ApJ*, 649, 722
- Weedman, D. et al. 2006, *ApJ*, 653, 101
- Weiner, B. J. et al. 2007, *ApJ*, 660, L39
- Williams, R. E. et al. 1996, in *Science with the Hubble Space Telescope - II*, ed. P. Benvenuti, F. D. Macchetto, & E. J. Schreier, 33–+
- Willmer, C. N. A. et al. 2006, *ApJ*, 647, 853
- Yan, L. et al. 2007, *ApJ*, 658, 778
- Yan, R., White, M., & Coil, A. L. 2004, *ApJ*, 607, 739
- Yang, X., Mo, H. J., van den Bosch, F. C., Pasquali, A., Li, C., & Barden, M. 2007, *ArXiv e-prints*, 707
- Zehavi, I. et al. 2002, *ApJ*, 571, 172
- Zheng, X. Z., Dole, H., Bell, E. F., Le Floch, E., Rieke, G. H., Rix, H.-W., & Schiminovich, D. 2007, *ArXiv e-prints*, 706

	LIRGs and ULIRGs	All galaxy	All galaxy - IR
no selection	33%	27%	25.5%
Monte Carlo results		1%	0.1%
(U-B) selected	29%	25%	23%
Monte Carlo results		13%	2%
M_B selected	32%	28%	26%
Monte Carlo results		13%	3%
Mass selected ¹	32%	32%	30%

Table 4: Fraction of sources being classified as group members as a function of color, luminosity and mass for the “LIRG and ULIRG” sample and the complete sample of sources with $0.7 \leq z \leq 1$.

Comments : (1) No Monte Carlo results are given since no trends are seen.